HARNESSING MESENCHYMAL STEM CELL EXOSOMES AS THERAPY FOR FIBROTIC LUNG DISEASE-INDUCED RIGHT VENTRICULAR DYSFUNCTION

by

Joel Munakwa Njah

GCE A Level, NCC Bamenda, Cameroon, 1986

MD, University of Yaoundé 1-Cameroon, 1994

MPH, University of Pittsburgh, 2010

Submitted to the Graduate Faculty of

School of Medicine in partial fulfillment

of the requirements for the degree of

Doctor of Philosophy

UNIVERSITY OF PITTSBURGH

SCHOOL OF MEDICINE

This dissertation was presented

by

Joel Munakwa Njah

It was defended on

July 20, 2018

and approved by

Galen Switzer, PhD, Professor, Medicine

Luis Ortiz, MD, Professor, Environmental & Occupational Health

Yoel Sadovsky, MD, Distinguished Professor, OBGYN-Reproductive Sciences

Douglas Landsittel, PhD, Professor, Medicine and Biostatistics

Dissertation Director: Luis Ortiz, Professor, Environmental & Occupational Health

HARNESSING MESENCHYMAL STEM CELL EXOSOMES AS THERAPY FOR FIBROTIC LUNG DISEASE-INDUCED RIGHT VENTRICULAR DYSFUNCTION

Joel M. Njah, PhD

University of Pittsburgh, 2018

Idiopathic pulmonary fibrosis (IPF) is a fatal disease of unknown etiology with no effective treatment except for lung transplantation. It is characterized by progressive lung fibrosis leading to respiratory failure. Outcomes are worse with comorbidities such as right ventricular systolic dysfunction (RVSD) and pulmonary hypertension (PH). Consequently, there is an urgent need for novel treatment approaches for IPF. This dissertation aims to (1) determine the strength of the association between hemodynamic indices of right ventricular function and survival in IPF, (2) evaluate the therapeutic potential of human bone-marrow derived mesenchymal stem cells (hMSCs) and their derived exosomes in regulating the right ventricular function in a mouse model of IPF, and (3) categorize the protein cargo of hMSCs.

The analysis of the data from an IPF registry showed that the risk of death was significantly higher among subjects with PH in IPF compared to IPF alone (HR: 1.406; 95% CI: 1.026-1.928). Similarly, the risk of mortality was significantly higher in subjects with RVSD compared to those without (HR: 2.523; 95% CI: 1.599-3.979). We concluded that PH and RVSD were strongly associated with survival and that right heart catheterization hemodynamic

assessments in IPF is crucial to identify patients at risk of worse outcomes who may be considered for clinical trials.

In evaluating the potential beneficial effects of hMSC and their exosomes in fibrotic lung injuries, we found that the mean pulmonary arterial pressure was significantly increased in the BLM group when compared with controls (20.0±0.45 vs 16.1±0.43, mmHg). Also, there was a significant increase in right ventricular dysfunction (dP/dtmx-EDV) when comparing the BLM group with controls (45.5±2.52 vs 32.8±2.87, mmHg.s-1. ul-1) with an improvement in the RVD after administering hMSCs and exosomes. We concluded that hMSCs and their exosomes have the therapeutic potential to regulate the RV contractile function.

Lastly, we performed a descriptive proteomic analysis to identify and categorize the protein components of the hMSC exosomes. We identified 845 proteins, 166 of them had enzymatic activities involved in proteolysis and oxidative stress regulation. Our conclusion was that the proteome of hMSC exosomes carry enzymatic proteins that could mediate their therapeutic effects.

TABLE OF CONTENTS

LIST OF TABLES

LIST OF FIGURES

PREFACE

This PhD dissertation is dedicated to my beloved late sister, Lucy Eni Munakwa, who passed away from a malignant tumor in September 2016. Sister, you inspired me to keep fighting even when the odds are not in our favor.

This has been a long academic journey with many bumps along the way and encountering many wonderful people who have lifted me up and encouraged me to forge ahead. I will like to start by thanking my Almighty Creator for giving me the good health and strength to tackle this challenging but rewarding endeavor. This work would not have been possible without the constructive comments, suggestions and insightful inputs from my committee members that have advanced my knowledge and skills in generating a scientific article. I want to specially recognize and thank my mentor Dr. Luis Ortiz who introduced me into the field of basic biomedical research and provided the platform to conduct this work. Your human touch to our personal relationship has been a blessing to my personal growth as a person and a scientist. To Dr. Galen Switzer, my academic advisor, for his continuous guidance and encouragement from the first day I met him as a new PhD student.

This work certainly would have been difficult to accomplish without the assistance of Mr. Elan Cohen at the University of Pittsburgh Data Center for his assistance in cleaning and coding part of the data for statistical analysis. Dr. George Leikauf and Dr. James Fabisiak for their assistance and guidance with the proteomic and KEGG pathway analysis. Dr. Berthony

Deslouches and Dr. Kiflai Bein for generously proofreading this work. To my laboratory colleagues, present and past, Dr. Michelangelo DiGiuseppe, Brian Brockway, Dr. Antonella Marrocco and Ariana Detwiler for their assistance and friendly support on numerous occasions over the years. I will like to acknowledge the personnel at the Vascular Medicine Institute and Biomedical Mass Spectrometry Center at the University of Pittsburgh for conducting the pressure-volume loop and proteomic analysis, respectively.

Finally, I will forever be grateful to my loving and caring wife, Vivian, and our three wonderful kids, Marielle, Belisse and Joevi for their continued love and tireless support despite my never-ending quest for knowledge. To my dear sisters and their amazing husbands, Mrs. Grace Tekum and Mrs. Mercy Tebit, words cannot describe the impact of your unwavering affection and prayers on my drive to succeed. I thank you all immensely.

1.0 INTRODUCTION

1.1 EPIDEMIOLOGY OF IPF

Idiopathic pulmonary fibrosis (IPF) is a debilitating and fatal disease of unknown etiology with no effective cure except for lung transplantation. It is characterized by progressive lung fibrosis leading to difficulties in breathing and a short median survival of 3-5 years [1]. The estimated prevalence of IPF in the United States is between 28 to 63 cases per 100,000 persons with about 50,000 annual incident cases [2, 3]. Despite the unpredictable course of IPF, outcomes are worse with an associated right ventricular (RV) dysfunction (RVD) and pulmonary hypertension (PH) [4, 5].Consequently, there is an urgent need for novel treatment options for IPF and its comorbidities.

1.2 AIMS AND RATIONALE

In this dissertation we tried to achieve three aims in three independent projects. Our first aim was to determine the strength of the association between hemodynamic indices of RVD and survival based on data from an IPF registry. For a rare disease such as IPF with a short median survival, a registry with structured data entry spanning several years will be a good resource to gather sufficient data to address this question. We hypothesized that patients with PH in IPF will have increased rates of RVD and poorer survival. In the second aim, we sought to evaluate the role of

hMSC and their derived exosomes in modulating the RV function in an experimental animal model of fibrotic lung injury. There is accumulating evidence on the beneficial effects of bone marrow-derived human mesenchymal stem cells and their secreted exosomes in fibrotic lung diseases and RV function [6-8]. A greater impetus is therefore needed to rapidly translate this promising novel therapeutic strategy into clinical applications. In view of this, we sought in our second aim to evaluate the role of hMSC and their derived exosomes in modulating the RV function in an experimental animal model of fibrotic lung injury. We hypothesized that hMSCs exosomes exert their beneficial effects in part, by modulating RV contractility. Lastly, in our third aim, we sought to identify and categorize the protein components of hMSC exosomes by a qualitative proteomic analysis. We questioned if the observed beneficial effects of hMSC exosomes could be partly explained by the composition of their protein cargo. These three aims are conceptualized in the conceptual framework below. The biogenesis of EVs is key to understanding the subcellular origins of extracellular vesicles that may in part, explain the differences in the protein cargo of microvesicles, budding from the plasma membrane and exosomes that originate from mature intracellular endosomal multivesicular bodies.

1.3 COMORBIDITIES ASSOCIATED WITH SURVIVAL IN IPF

The correlation between RVD and survival has been widely reported based on studies conducted in patients with idiopathic pulmonary arterial hypertension (IPAH) [9, 10]. Nonetheless, there is a critical difference in the definition of IPAH and pulmonary hypertension in IPF (PH in IPF). Therefore, motivated by the need to highlight these differences and harmonize the diagnosis and treatment of PH, a series of world symposia were held under the sponsorship of the World

Health Organization since 1973 to the latest in 2013 [11, 12]. The robust discussions during these symposia led to a clear definition and classification of PH. Consequently, PH in general, is defined as a hemodynamic and pathophysiological condition with an increase in mean pulmonary arterial pressure (mPAP) ≥25 mmHg at rest, assessed by right heart catheterization (RHC). Idiopathic pulmonary hypertension was classified as a group 1 PH, which is characterized by the presence of pre-capillary PH in the absence of other causes of pre-capillary PH. PH in IPF was classified as a group 3 precapillary PH due to lung diseases or hypoxia. To differentiate PH in IPF from the group 2 postcapillary PH due to left-sided heart disease, a second hemodynamic parameter in the diagnosis of PH in lung diseases was introduced. This was a pulmonary capillary wedge pressure (PCWP) ≤15 mmHg [12]. Several studies comparing hemodynamic parameters and survival of patients with precapillary PH (group 1, IPAH and group 3, PH in IPF), suggest a direct correlation between pulmonary hypertension and poor survival [13-15]. Put together, these studies suggest that treating PH alone may prolong survival in IPF. Nonetheless, the updated American Thoracic Society (ATS)/European Respiratory Society (ERS) clinical practice guidelines of 2015, maintained the 2011 guidelines against treating PH in IPF [16]. They argued that the current vasoactive therapies for IPAH are more likely to worsen the already compromised gas exchange in IPF patients. Pulmonary functional tests (PFTs) are often conducted to assess disease progression based on lung volumes with forced vital capacity percent predicted (%FVC) and gas exchange with diffusion capacity for carbon monoxide percent predicted (%DLco) [17]. Clinically significant reductions in FVC and DLco that correlate with increased mortality have been shown to be greater than 10% and 15%, respectively [18]. Recently, Paterniti M. et al, studying the PFTs of placebo subjects in the nintedanib-INPULSIS 1/2 and pirfenidone-CAPACITY 004/006, ASCEND clinical trials, found that subjects with less than

55% and 36% of %FVC and %DLco, respectively, had the highest risk of death [19]. Collectively, the results from these clinical trials led to the approval of pirfenidone and nintedanib in the treatment of IPF, based on reductions in the decline of the % predicted FVC but with little or no improvements in mortality [19]. Therefore, other factors that correlate strongly with mortality are needed for optimal patient management.

1.3.1 Pulmonary hypertension in IPF

Patients suffering from IPAH are reported to be dying mostly from the failing right ventricle [20]. Until recently, the right ventricle was considered a bystander conduit for blood to the lungs but advances in studying PH have generated interest in understanding its adaptative role in pulmonary pressure overloads [21]. Therefore, based on the accumulating evidence on the importance of the right ventricle in PH, the NHLBI working group on the molecular and cellular mechanisms of RV failure, published a 2006 report emphasizing the need to assess the RV function in relation to cardiopulmonary diseases, including PH in IPF [20]. Consequently, Vonk Noordegraaf and others have proposed a progressive adaptation of the right ventricle, from RV hypertrophy (to maintain RV to pulmonary arterial coupling) to RV dilatation that results in uncoupling or overt RV failure [10, 22]. These adaptational steps are reported to begin with an increased RV contractility and myocardial hypertrophy, followed by progressive contractile dysfunction due to maladaptive RV dilation [4, 23, 24]. The failing RV is therefore, characterized by an initial increase in contractility followed by a progressive weakening in contractility as the RV afterload overcomes contractility [25, 26]. Validated indicators of RVD are therefore, essential in assessing the transition from adaptive (increased RV contractility) to maladaptive (RV dilatation) RVD and in determining how they correlate with survival in IPF.

1.3.2 RVD in IPF

Different hemodynamic indices of RVD and PH have been shown to have various prognostic values and strength of association with survival. Wauthy and associates, investigating RV-pulmonary arterial uncoupling (failing RV) in large animal models, demonstrated that survival was strongly associated with RV systolic dysfunction (RVSD) than with elevated pulmonary artery pressures [27]. These authors defined uncoupling as the inability of the RV to maintain a normal stroke volume with increased pulmonary pressure overload. This report indicates indices of RVSD might have better prognostic values than pulmonary pressures when appropriate modalities are used for its assessment.

1.4 MOUSE MODEL OF IPF

Currently, there is no effective treatment for IPF and the recently approved pirfenidone and nintedanib, at a prohibitive cost only help in slowing IPF progression. It is therefore, imperative to translate evidence-based findings from preclinical animal models into clinical applications that have the potential to treat IPF and improve survival. Animal models of IPF and its comorbidities are crucial in studying the pathogenesis of IPF and their response to treatment. Mouse bleomycin (BLM) pulmonary fibrosis model is an established model that has been useful in elucidating major aspects of our current knowledge on IPF. Bleomycin is a glycopeptide antibiotic produced from the bacteria, Streptomyces verticillus. It has traditionally been used as a cytotoxic agent in cancer chemotherapy based on its properties of inducing oxidative DNA breakage [28, 29]. The initial histopathological lung injury associated with BLM, recapitulates human IPF with either

peribronchiolar or subpleural basal lesions depending on whether it was administered intratracheally or subcutaneously, respectively [30]. BLM-induced fibrotic lung injury (BFLI) in rodent models has been shown to be associated with pulmonary hypertension (PH)[30]. Therefore, as in human IPF where the outcome is often complicated by right ventricular (RV) dysfunction (RVD) and PH [5, 15] , these comorbidities are likely to be present in animal models of BFLI. Using a mouse model of BFLI, Hemnes A et al, reported an improvement in pulmonary vascular remodeling and RV hypertrophy after administering sildenafil, a selective phosphodiesterase type 5 (PDE5) inhibitor [30]. This study and others confirmed the use of the mouse BLM-induced model as an ideal model to study the beneficial effects of hMSCs in BFLI [31].

1.5 THE THERAPEUTIC POTENTIAL OF HMSCS AND THEIR EXOSOMES

Mesenchymal stem/stromal cells (MSCs) are multipotent cells that have the capacity for self-renewal and differentiation into multiple lineages, including adipocytes, chondrocytes, and osteocytes [32]. They were first discovered by Friedenstein and colleagues in the late 1960s as cells from the bone marrow which adhere to plastic with a fibroblastoid shape [33, 34]. Since then, there has been a dramatic increase in the number of published articles on the therapeutic potential of hMSCs in different disease conditions, particularly in pulmonary fibrosis [35, 36]. Though most of the over 10,000 reports from preclinical trials on their beneficial effects have been on bone marrow-derived MSCs, these cells have now been isolated from nearly every tissue, including fat, umbilical cord, placenta and embryonic stem cells [33, 37, 38]. An updated review by Squillaro et al showed that since June 2015, there were 493 reported MSC-based clinical trials. Of these, 23 (4.8%) involved lung diseases and 73 (14.8%) cardiovascular diseases [39]. Unfortunately, these

published reports had major discrepancies in the definition and characterization of MSCs, prompting the International Society for Cellular Therapy (ISCT) in 2006, to propose minimal criteria for defining hMSCs: hMSCs must be plastic-adherent in culture; positive for CD105, CD90, CD73; negative for CD45, CD34, CD11b, HLA-DR surface markers and lastly, must differentiate into osteoblasts, adipocytes and chondroblasts [32]. These minimal standards have led to improvements in the consistencies in the methods used to isolate and expand MSCs. Nonetheless, there is still the need for biomarkers that can quantitatively delineate high quality, therapeutic potent MSCs [40, 41]. Recent animal studies have shown a correlation between the therapeutic potential of allogeneic hMSCs with the dose and timing of their transplantation [33, 42]. Most of these studies have confirmed the efficacy of MSCs early during the inflammation phase and not after established FLI [33, 43]. Unfortunately, due to the insidious nature of the onset of IPF, most patients present late in hospitals with established progressive lung fibrosis, thus questioning the translation potential of the observed pre-clinal benefits, during the acute inflammatory phase, to clinical trials on patients with established chronic lung fibrosis. Furthermore, the efficacy of these cells is also associated to the lack of homogeneity of the transplanted hMSCs. The heterogeneity of MSC populations during isolation and their expansion in culture has raised concerns among investigators because of the likelihood of variations in their therapeutic potency. Therefore, reproducible, standardized protocols for the isolation and expansion of clonal MSCs in culture are needed to produce homogeneous cell populations with predictable potency [43]. To this end, biomarkers to predict the potency of MSCs from different donors will be necessary to translate their ameliorating effects from preclinical animal models into clinical applications [40, 41]. However, the role of endogenous stem cells/progenitor cells in tissue repair and how they interact with exogenous injected MSCs is still not fully understood [33, 44]. It will be crucial to

delineate the relative contributions of exogenous from endogenous stem cells in FLI repairs. Even though the mode of actions of MSCs remain poorly understood, the paracrine concept as a mechanism employed by MSCs to impart their beneficial effects is increasingly recognized, in part by their release of EVs [33, 45, 46].

1.5.1 Human mesenchymal stem cell-released exosomes

Mesenchymal stem cells release membrane-bound vesicles that encompass exosomes and microvesicles (MVs). Exosomes (30-100nm) originate from mature endosomal multi-vesicular bodies, while the larger MVs (0.1-1um) are formed by outward budding off the plasma membrane [47, 48]. Recent studies have shown that these EVs carry cytoplasmic nucleic acids (mRNA, microRNA), membrane proteins and lipids that are specific to the parent cell type and are mediators of the change in differentiation state of recipient cells or their reprogramming [45, 49]. Specifically, exosomes have been demonstrated to be enriched in microRNAs (miRs) and mRNAs, while MVs have little or no RNA, suggesting exosomes because of their endosomal origins might be better effectors of the beneficial MSC effects [46, 50]. Other studies suggest a synergistic mode of action of these EVs to exert pleiotropic beneficial effects in tissue repair [45], especially in modulating the RV function. Therefore, innovative techniques will be needed to accurately evaluate the adaptive changes in the RV function as a result of the increasing pulmonary pressure overload and their response to hMSC exosomes treatment.

1.6 RIGHT HEART CATHETERIZATION AND INDICES OF RVD

Right heart catheterization (RHC) and PV loop analysis remain the gold standard for defining changes in PH and assessing the hemodynamic load on the RV [4]. Recent studies indicate the changes in RV function begin prior to the setting in of overt PH [26, 51]. Furthermore, growing evidence suggest the RV adapts to increased afterload by increasing its wall thickness (hypertrophy) and contractility [4, 24]. When these adaptive compensatory mechanisms are overwhelmed by the increasing pulmonary pressure overload, RVD ensues and progressively lead to uncoupling of the RV from the pulmonary vasculature. Uncoupling has been defined as 'the inability of the RV to maintain a normal stroke volume with increasing pressure overload'. Wauthy and associates investigating RV-pulmonary arterial uncoupling in large animal models, found that worse survival was strongly associated to RV systolic dysfunction (RVSD) and not to the elevated pulmonary artery pressures [27]. Unlike PH with well validated and standardized indices for its assessment, there are no well standardized indices for assessing RVD. In an attempt to address the lack of standardized indictors for RVD, experts at the Fifth World Symposium on Pulmonary Hypertension held in 2013, adopted a definition of RV failure secondary to PH as, "a complex clinical syndrome due to a suboptimal delivery of blood or elevated systemic venous pressure at rest or exercise as a consequence of elevated RV afterload" [11].

1.7 THE POTENTIAL MECHANISTIC PATHWAYS OF HMSC EXOSOMES

There is accumulating evidence on the beneficial effects of hMSCs in a wide range of diseases, including fibrotic lung diseases and their induced pulmonary hypertension and right ventricular dysfunction. However, the underlying mechanisms by which hMSCs impart their beneficial effects are still actively being investigated. The fact that few MSCs engraft at the site of injury led to a shift in the concept of the potential pathways used in their ameliorating effects; from engraftment and differentiation, to replace damaged resident cell types, to the release of paracrine effectors [33, 52]. Insoluble extracellular vesicles are a major part of the hMSC paracrine secretome.

Mesenchymal stem cells release membrane-bound EVs that encompass exosomes and microvesicles (MVs). Exosomes (30-100nm in diameter) originate from mature endosomal multi-vesicular bodies, while the larger MVs (0.1-1um in diameter) are formed from plasma membrane blebs [48, 53]. Recent studies have shown that these EVs carry cytoplasmic nucleic acids (mRNA, microRNA), membrane lipids and proteins that are specific to their parent cell type and are potential mediators of changes in the differentiation state of recipient cells [45, 49]. Specifically, exosomes have been demonstrated to be differentially enriched in microRNAs (miRs), while MVs have little or no miRs, suggesting exosomes may be better mediators of the beneficial MSC effects [46, 50]. Other reports suggest a synergistic mode of action of these EV subtypes to optimize their pleiotropic beneficial effects in tissue repair [45].

Recently, we showed that MSCs exert their beneficial actions in part, by shuttling miRs and proteins loaded in EVs to target cells leading to a change in their bioenergetic phenotype [45]. Other investigators have shown that hMSC exosomes contribute to the ameliorating effects in myocardial infarction [54], pulmonary hypertension [55, 56], and pulmonary fibrosis [6, 37]. Collectively,

these studies suggest a potential cross-talk between hMSC exosomes and target cells, such as endothelial cells, cardiomyocytes, and lung epithelial cells for tissue repair. A greater understanding of the molecular and cellular pathways in the pathogenesis of RV and pulmonary artery remodeling in fibrotic lung diseases will help in the development of novel therapeutic strategies. To this end, some investigators have proposed mechanistic pathways that involve the generation of excessive reactive oxygen species (ROS) as crucial in the pathogenesis of fibrotic lung disease [57] and right ventricular hypertrophy [58]. Furthermore, others have postulated an increased expression of NADPH oxidase (NOX) and mitochondrial ROS production as key sources of ROS that correlate with progressive RV hypertrophy [59-61]. These data suggest a deleterious effect of oxidative stress on the normal function of the right ventricle and pulmonary vasculature that has triggered interest in the development of mitochondria-based therapy, such as MitoQ, to treat cardiac hypertrophy [62]. Importantly, oxidative stress is directly associated with an increase in misfolded proteins [63], which are toxic to cells as reported in a wide range of neurogenerative and age-related diseases such as IPF. The ATP-dependent proteolytic, 26S ubiquitin/proteasome system is crucial in recognizing and selectively degrading misfolded proteins [64, 65]. Proteolytic enzymes are therefore needed to clear these misfolded intracellular and extracellular proteins. Proteasomes are an essential group of hydrolase proteolytic enzymes that have been found in hMSC exosomes. According to Lai et al, proteasomes played an important role in the clearing of misfolded proteins to mitigate ischemia/ reperfusion (I/R) injury [66]. Taken together, these data indicate a pivotal role of proteasomes in the clearance of misfolded proteins with a potential proteolytic role in the extracellular matrix (ECM). Their proteolytic actions may have a synergistic effect with matrix metalloproteinases (MMP). The gelatinases (MMP2 and MMP9) are MMPs that have been shown to play an important role in ECM turnover and have

also been identified in MSC exosomes [67]. However, despite our current understanding of the role of antioxidant and proteolytic enzymes in health and disease, the hMSC exosome proteome has not been investigated to specifically identify these potential paracrine effectors.

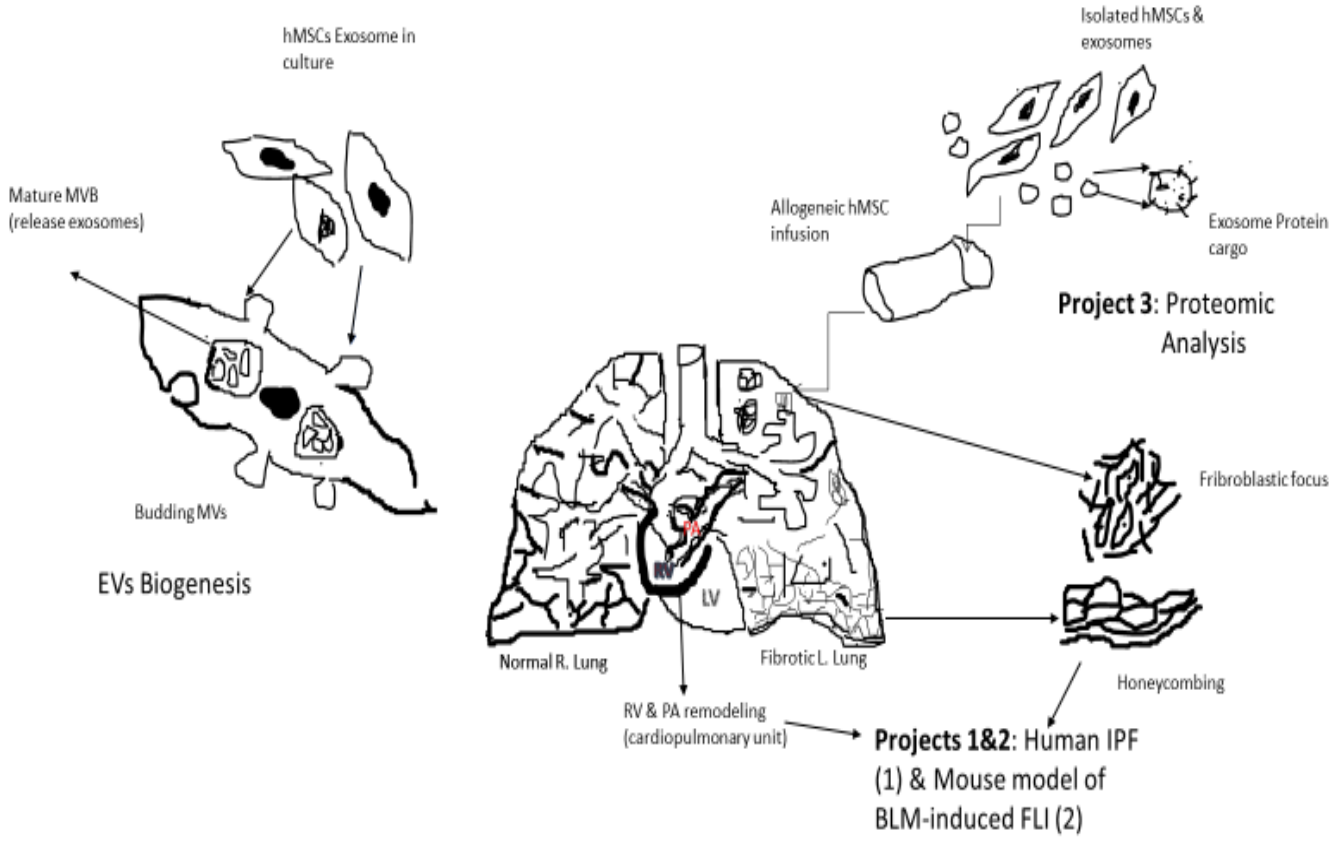

Figure 1 A conceptual framework integrating the three aims

.

2.0 HEMODYNAMIC CHARACTERISTICS OF SURVIVAL IN IPF: ANALYSIS FROM THE SIMMONS CENTER FOR INTERSTITIAL LUNG DISEASES REGISTRY

2.1 INTRODUCTION

Right ventricular dysfunction has been shown to directly correlate with worse survival in group 1 IPAH[4, 9]. Most of the studies on IPAH used doppler echocardiography to assess the RV function. Though noninvasive and suitable for follow-up assessments of patients, echocardiographic techniques have shown limited accuracy in measuring RV function in advanced lung diseases[5, 15]. Some reports have shown accuracy as low as 40% when compared with RHC measurements [68]. Furthermore, echocardiograms have the disadvantage that the parameters they measure are load-dependent and lack the ability to study the intrinsic properties of the right heart[69]. Notwithstanding, echocardiography has provided added insight into the adaptive changes in shape and size during right heart filling and output.

In 2013, Rivera-Lebron and colleagues used echocardiographic parameters, including tricuspid annular plane systolic excursion (TAPSE) as a measure of RV ejection fraction and RV outflow tract velocity-time integral (RVOT VTI) as a surrogate for stroke volume. They found that those with RVD in IPF had significantly lower TAPSE (1.8 cm vs 2.1 cm; P=0.01) [15]. Similarly, D'Andrea et al, used another echocardiographic technique, speckle-tracking (2D strain) echocardiography (2D STE) to quantify RV regional deformation and RV contractile

impairment in 55 IPF patients. They found a significant reduction in global longitudinal strain of IPF patients when compared with controls (−18.4 ± 6.1 vs −14.5 ± 6.3) [5]. Furthermore, Ghio et al, studying 658 consecutive patients with congestive heart failure, showed that a TAPSE ≤14 mm was more significantly associated with mortality than elevated pulmonary systolic pressure with preserved TAPSE. Put together, these echocardiographic studies reinforce the importance of TAPSE, a measure of RVD, as a strong prognosticator of survival. However, as earlier mentioned, echocardiography is fraught by limitations of delineating the endocardium for accurate evaluations of right-sided heart volumes. Thus, the need for invasive RHC and PV loop analysis (RHC-PV loop analysis).

Though minimally invasive, RHC-PV loop analysis is the gold standard for assessing the hemodynamic functions of the right heart [51]. PV loop analysis have become an essential tool in assessing disease progression and adaptation of the RV to the PH-induced increased RV afterload [22]. It is therefore, imperative to employ RHC to comprehensively study the pathophysiology of the failing RV and pulmonary vasculature and determine their association with survival However, there are currently no well-established indices for assessing RVD in IPF. PV loops generate end-systolic PV relationship slopes (Ees) that have been demonstrated to be load-independent [70]. Load-independent indices are crucial in assessing the intrinsic RV function void of the influence of load and heart rate [71]. Also, the interaction of the RV pump and pulmonary vascular load, RV-to-pulmonary arterial (PA) coupling, provides a comprehensive evaluation of the right ventricle and pulmonary circulation as a functional unit. PV loop analysis also, enable assessment of the RV contractility, especially with the evidence that the RV pump muscle shortening (contractility) and mass (hypertrophy) are essential elements that contribute to optimal RV function [21]. However, assessing the RV function in class 3 IPF-associated PH is

limited by the lack of well-established indices [72]. Recently, Rivera-Lebron and colleagues employed transthoracic echocardiography with stroke volume index (SVI) ≤29ml/m² as the cutoff for assessing RVD in IPF patients with associated PH [15]. More than a decade ago, van Wolferen and colleagues reported on the use of right ventricular systolic dysfunction (defined as low stroke volumes (≤25ml/m²) in predicting mortality in subjects with pulmonary arterial hypertension [9].Therefore, based on these reports we used a threshold level of (SVI≤25ml/m²) to assess the RV function in our IPF cohort.

In this regard, an IPF registry will be an important resource for large epidemiological data on real-world characteristics and clinical management of IPF patients [73-75]. In a recent publication from the Australian IPF registry evaluating baseline characteristics of IPF patients, forced vital capacity (FVC), diffusing capacity of the lung for carbon monoxide (DLco), composite physiological index (CPI) and GAP (gender, age, physiology) were found to be strong predictors of mortality [74]. Similarly, in a report from the INSIGHTS-IPF registry from Germany, the mean FVC was 72±20% predicted and DLco was 35±15% predicted [75]. Other regional or statewide registries such as the Swedish IPF-Registry have showed that the quality of life of IPF patients and their perception of the disease were quite poor [76]. Collectively, these studies indicate IPF registries are an important source for data on the natural history of the disease, quality of life and clinical management of patients.

Consequently, using hemodynamic data from the Simmons Center for interstitial lung diseases (ILDs) registry, we sought to use PV loop analysis to assess RV function and determine the strength of their association with survival in IPF patients. We hypothesized that IPF subjects with RVD will have worse survival when compared with those with PH in IPF and IPF alone.

2.2 METHODS

2.2.1 IPF registry

The Simmons Center for interstitial lung diseases (ILDs) registry at the University of Pittsburgh, was launched in October 2003 to document medical information from previously and newly diagnosed patients with ILDs, including IPF (ClinicalTrials.gov identifier #: NCT00258583). The center currently follows over 1400 patients with interstitial lung diseases, most with IPF. The center provides comprehensive state-of-the-art care for patients with interstitial lung diseases, opportunities for research on lung inflammation and fibrosis, and promotes the translation of scientific discoveries into novel therapies, such as stem cells and their derivatives. In 2008, the Simmons Center ILDs registry became a member of the Daniel and Joan Beren Pennsylvania-statewide IPF (PA-IPF) registry. The PA-IPF registry comprise five participating centers that include the University of Pittsburgh, University of Pennsylvania, Temple University, Penn State Hershey Medical Center, and Geisinger Health System. The data for this study came solely from the Simons Center registry, including doppler echocardiographic, demographic, pulmonary functional tests (PFTs) and right heart catheterization (RHC). Patients were determined to have IPF according to the 2002 ATS/ERS guidelines [77]. These guidelines were later revised in 2011 [1] and 2015 [16].

2.2.2 Data collection

Approval for the study (Protocol 13080573) was obtained from the University of Pittsburgh Institutional Review Board. The registry was reviewed for patients diagnosed with IPF from

between June 1996 to June 2015 to collate deidentified demographic and hemodynamic data into electronic spreadsheets. Thereafter, the secondary raw data was cleansed, categorized and assigned analytical variable codes with assistance from the University of Pittsburgh Center for Research on Health Care Data Center. Patients diagnosed with other diffused interstitial lung diseases, who did not meet the 2002 guidelines for IPF were excluded from the study.

2.2.3 Sample size and power analysis

The sample size (308) is determined from the number of patients diagnosed with IPF with RHC-derived hemodynamic data. However, we needed a power analysis to confirm an adequate sample size to detect a clinically meaningful difference in the survival probabilities between IPF alone and PH in IPF groups. The minimal sample size of 92 for 41 events (deaths) was determined to be adequate to detect a 30% difference in mortality between IPF alone and PH in IPF subjects. The log-rank test, assuming a chi-square distribution, was used to calculate the sample sizes [78] with the "power" command on a STATA software (Stata Corp., College Station; version 14.0). Null hypothesis H_0: $S_1(t)=S_2(t)$; Alternative H_1: $S_1(t)\neq S_2(t)$; where $S_1(t)$= survival probability in the IPF alone group, $S_2(t)$= survival probability in the PH in IPF group. The effect size of 30% was consistent with mortality rates reported by Lettieri and colleagues who compared the risk of mortality in IPF patients with PH and those without PH [79]. The sample size was calculated with a power (1-β) of 80%, a type II error (β) of 20% and a significance level of less than 0.05.

2.2.4 Statistical analysis

All statistical analyses were performed using a STATA statistical software (Stata Corp., College Station; version 14.0). Summary statistics for demographic, pulmonary function tests, and hemodynamic characteristics were evaluated. The data were reported as mean ± SEM or as median where appropriate and ccategorical variables were summarized as percentages. Comparisons of groups were made using unpaired Student t-test, Chi X^2 or Wilcoxon's rank-sum tests (see Table 1).

For survival analyses, unadjusted survival functions of dichotomized continuous variables of PH in IPF ($25 < mPAP \geq 25$) and SVI ($25 \leq SVI > 25$) were estimated using Kaplan-Meier curves with their log-rank test for statistical significance. Unadjusted and multivariable Cox proportional hazard analyses were performed, adjusting for key predictor variables (age, gender, heart rates and FVC% predicted). Other clinically meaningful variables were fitted one after the other in a model with the above key variables to evaluate the magnitude and significance of their association with mortality. A log-log plot was generated to test for the proportional hazard assumption. It is worth noting that the test of multicollinearity is inherent in the STATA software program. Associations between continuous variables were evaluated using Pearson's correlation test and logistic regressions were performed to evaluate the strength of the association between dichotomous variables. The dichotomized predefined threshold values of mean pulmonary arterial pressure (mPAP) (≥ 25 and PCWP ≤ 15 mmHg) and stroke volume index (SVI) (≤ 25 ml/beat/m^2) were evaluated for the presence of pulmonary hypertension or right ventricular systolic dysfunction, respectively. The p-value (< 0.05) and their 95% confidence intervals (CI) were assessed. for statistical significance. The 95% CI is not assessed for significance – it's additional information.

2.2.5 Primary endpoint

The primary endpoint was overall mortality, assessed by a Cox regression analysis and the secondary endpoint was prevalence. Other covariates evaluated were PVR (pulmonary vascular resistance), RVSP (right ventricular systolic pressure), and the predicted FVC% (forced vital capacity % predicted), FEV1% (forced expiratory volume in one second % predicted), DLco% (diffusion capacity for carbon monoxide % predicted) (Table 1). The proportion of missing data was small and did not affect our sample size calculations, thus allowing for a complete case analysis. Most of the missing data resulted from some subjects missing data points on either PFTs or RHC that could not be matched.

2.3 RESULTS

2.3.1 Study population

We identified 880 patients with IPF in the review period from June 1996 to June 2015. Of these, 308 (35%) had complete hemodynamic and PFTs data. Sixty five percent of the IPF patients that were not analyzed had a similar demographic distribution (age, race) with a slight reduction in the proportion of males (57% vs 67%) when compared with the analyzed data.

2.3.2 Demographics

The overall mean age of the analyzed IPF cohort was 68 years (range 31 to 94) and 67% male. The cohort was mostly white, with 836 (95%) followed by African Americans, 18 (2%) and others 26 (3%). The PH in IPF subjects comprised mostly older males when compared with IPF

only subjects (66 vs 64; p=0.05). The prevalence of PH and RVSD in IPF were 28.6% (88/308) and 12.3% (28/228), respectively (Table 1 & 2).

Table 1. Characteristics of IPF patients with IPF alone and PH in IPF

Unit: mmHg	IPF alone (<25) (n = 220)	PH in IPF (≥25) (n = 88)	P-value
Demographics			
Age, yrs	63.9 ± 0.6	65.9 ± 0.9	0.05$^{\Phi}$
Gender, male, n (%)	141 (45.8)	65 (21.1)	0.1$^{\text{m}}$
Race/ethnicity			0.04$^{\Phi}$
White, n (%)	214 (69.5)	82 (26.6)	
African American, n (%)	2 (0.01)	6 (0.02)	
Hispanic, n (%)	2 (0.01)	0 (0)	
American Indian, n (%)	1 (0)	0 (0)	
Others, n (%)	1 (0)	0 (0)	
Pulmonary Function Test			
FVC, % predicted	60.1 ± 1.3	58.6 ± 2.1	0.55$^{\Phi}$
FEV1, % predicted	68.6 ± 1.4	66.6 ± 2.2	0.45$^{\Phi}$
DLCO, % predicted	38.7 ± 1.5	30.5 ± 1.6	<0.001$^{\Psi}$
Right Heart Catheterization			
mPAP, mmHg	21.8 ± 0.6	35.8 ± 1	<0.001$^{\Psi}$
RVSP, mmHg	38.8 ± 0.9	59.2 ± 1.8	<0.001$^{\Psi}$
RVDP, mmHg	2.6 ± 0.4	3.7 ± 0.6	0.119$^{\Phi}$
HR, bpm	76.1 ± 1.5	77.3 ± 2.2	0.58$^{\Phi}$
CO, L/min	5.4 ± 0.1	4.9 ± 0.15	0.005$^{\Phi}$
CI, L/min/m^2	2.8 ± 0.05	2.5 ± 0.07	0.005$^{\Phi}$
SV, mL/beat	76 ± 1.9	67.1 ± 2.9	0.01$^{\Phi}$
SVI, mL/m²/beat	38.9 ± 0.9	34.1 ± 1.3	0.003$^{\Phi}$
PCWP, mmHg	10.6 ± 0.4	9.2 ± 0.4	0.51$^{\Psi}$
TPG, mmHg	10.9 ± 0.4	26.8 ± 1.1	<0.001$^{\Psi}$
PVR, WU	2.2 ± 0.1	6 ± 0.4	<0.001$^{\Psi}$

Frequency (n) and percentage (%) ± sem; FVC: Forced vital capacity; FEV1: Forced expiratory volume in one second; DLCO: Diffusion capacity of the lung for carbon monoxide; mPAP: Mean pulmonary arterial pressure; RVSP: Right ventricular systolic pressure; RVDP: Right ventricular diastolic pressure; HR: Heart rate;CO: Cardiac output; CI: Cardiac index; SV: Stroke volume; SVI: Stroke volume index; PCWP; Pulmonary capillary wedge pressure; TPG: Transpulmonary pressure gradient; PVR: Pulmonary vascular resistance; WU: Wood unit; Chi2 test $^{\text{m}}$, rank-sum test$^{\Psi}$, t-test$^{\Phi}$.

2.3.3 Pulmonary functional tests

There were no significant differences in the mean FVC % and FEV1% predicted values between the PH in IPF and IPF only groups, confirming previous reports that lung volumes do not correlate well with patient outcomes [13]. The DLCO % predicted was significantly lower in the PH in IPF group (30.5 vs 38.7, p= <0.001) (Table 1).

Table 2 Characteristics of patients with RVSD and preserved RV function

Unit: ml/beat/m²	SVI (>25) (n = 200)	SVI (≤25) (n = 28)	P-value
Demographics			
Age, yrs	64 ± 0.6	67 ± 0.6	0.03Φ
Gender, male, n (%)	127 (55.7)	18 (7.9)	0.94ᵐ
Race/ethnicity			0.002Φ
White, n (%)	197 (86.4)	25 (11)	
African American, n (%)	1(0)	3 (1.3)	
Hispanic, n (%)	1 (0)	0 (0)	
Others, n (%)	1 (0)	0 (0)	
Pulmonary Function Test			
FVC, % predicted	69.8 ± 1.5	62.5 ± 3.9	0.08Φ
FEV1, % predicted	61.7 ± 1.4	53.4 ± 3.5	0.04Φ
DLCO, % predicted	38 ± 1.5	33 ± 4	0.22Φ
Right Heart Catheterization			
mPAP, mmHg	24 ± 0.7	36 ± 2.8	<0.001Ψ
RVSP, mmHg	44 ± 1.1	60 ± 4.3	0.001Ψ
RVDP, mmHg	1.9 ± 0.3	4.5 ± 1.4	0.033Ψ
SVI,mL/m²/beat	40 ± 0.7	20 ± 0.8	<0.001Ψ
HR, bpm	72 ± 1	103 ± 6	<0.001Ψ
PCWP, mmHg	10 ± 0.4	10 ± 1.4	0.78Ψ
TPG, mmHg	14 ± 0.6	26 ± 2.8	<0.001Ψ
PVR, WU	2.8 ± 0.1	7.5 ± 1	<0.001Ψ

Forced vital capacity; FEV1: Forced expiratory volume in one second; DLCO: Diffusion capacity of the lung for carbon monoxide; mPAP: Mean pulmonary arterial pressure; RVSP: Right ventricular systolic pressure; RVDP: Right ventricular diastolic pressure; HR: Heart rate; PCWP; Pulmonary capillary wedge pressure; TPG: Transpulmonary pressure gradient; PVR: Pulmonary vascular resistance; WU: Wood unit; Chi2 test ᵐ, rank-sum testΨ, t-testΦ.

2.3.4 Survival analysis

The overall median survival was 3.7 years, and the 1-year and 5-year survival rates were 81.3% and 37.5%, respectively (Figure 1). This showed a rapid decline (43.8%) in survival from one to five years after diagnosis. The assumption of constant proportional hazard was determined to be satisfactory from a parallel log-log graph.

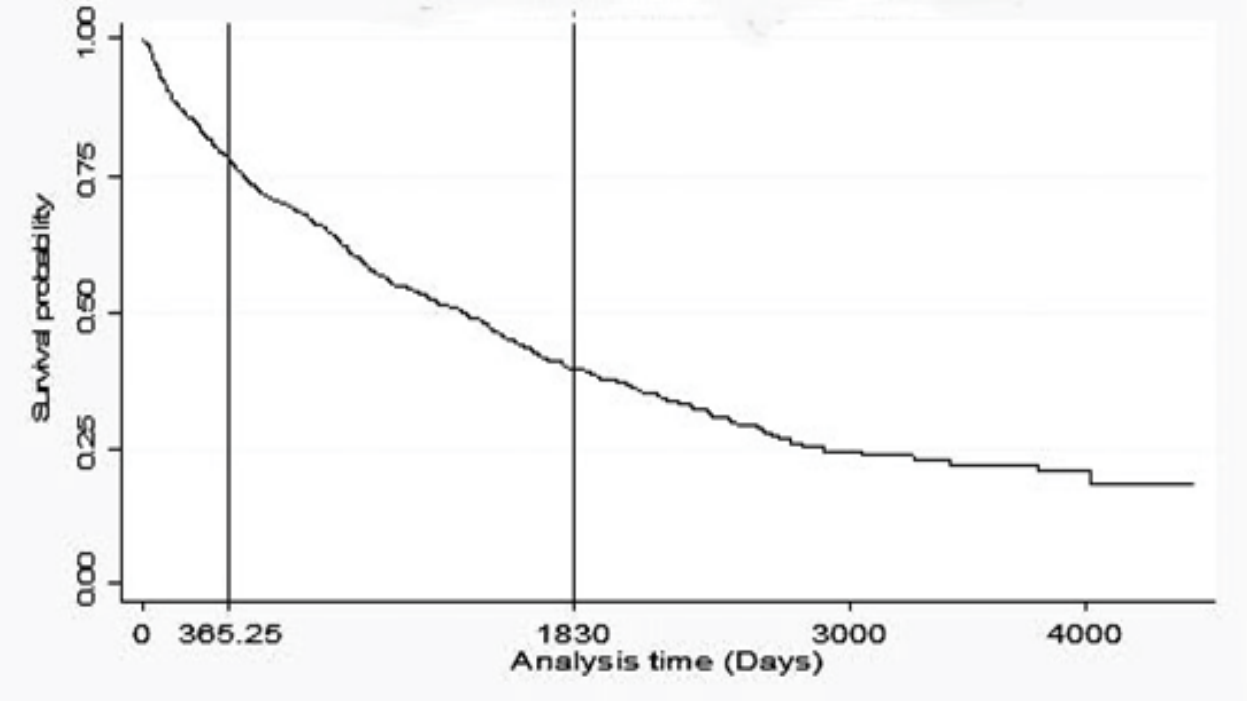

Figure 2 Overall survival curve with a decline from 1 (365.25) to 5 (1830) years following diagnosis

In comparing the Kaplan-Meier survival estimates (Figure 2A), we found a significantly lower survival rate among PH in IPF subjects compared with IPF alone. Furthermore, the survival estimates were significantly lower in the PH-IPF group at one year (72.3 % vs 85.3%) and at five years (37.9% vs 49.6%) than in IPF alone. This suggest a worsening survival outcome attributable to PH in IPF. Looking at RV function, the Kaplan-Meier survival estimates of subjects with RVSD were significantly lower at one year (67.2% vs 83.7%) and at five years (16.8% vs 55.4%) compared to those without RVSD (Figure 2B). Interestingly, these rates were 5% and 21% lower at one year and five years respectively, among RVSD subjects compared

with PH in IPF. This indicate outcomes are markedly worse in IPF patients with associated RVSD when compared with PH in IPF.

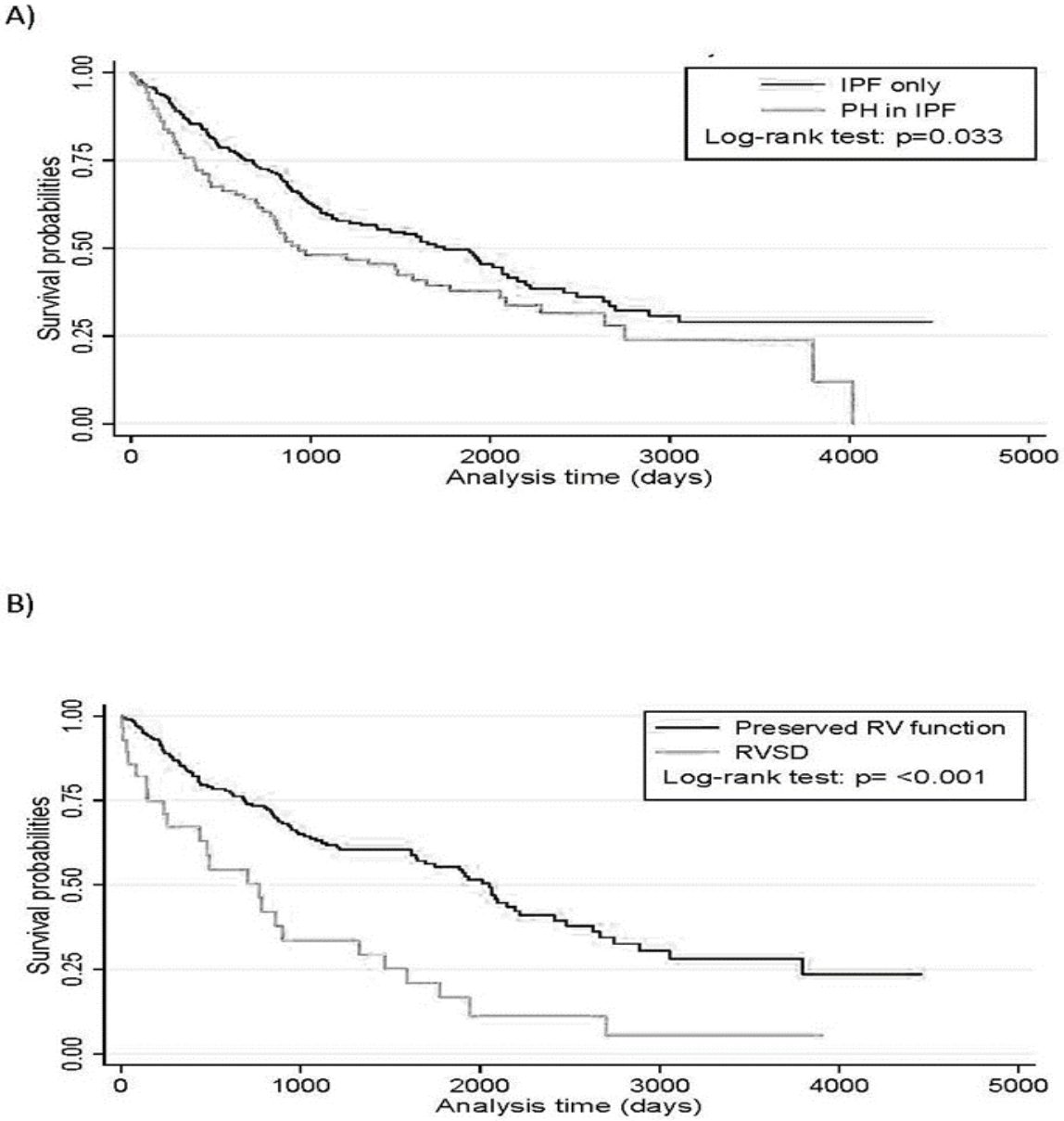

Figure 3 KM survival estimates. (A) PH in IPF vs IPF alone (B) RVSD vs preserved RV function

2.3.5 Cox proportional hazard regression analysis.

2.3.5.1 Unadjusted analysis

To assess the impact of PH in IPF on survival outcomes, we performed an unadjusted Cox regression analysis with a dichotomized mPAP (mean pulmonary artery pressure) as a single covariate. The overall risk of mortality (hazard ratio) was significantly higher among subjects with PH in IPF compared to IPF alone (HR: 1.406; CI: 1.026-1.928, p= 0.034). More importantly, the risk of death was significantly higher in subjects with RVSD compared to those without. (HR: 2.523; 95% CI: 1.599-3.979, p= <0.001) (Table 2). Again, RVSD in IPF was associated a greater risk of death than PH in IPF. Interestingly, the significant different variables (mPAP, RVSP) are indicators of pulmonary vascular load (afterload) related to the cardiopulmonary functional unit.

Table 3 Cox proportional hazard for overall mortality in RVSD and PH in IPF

	PH-IPF (≥25 mmHg)		RVSD (SVI ≤25 ml/beat/m²)	
Cox regression analysis	**HR (95% CI)**	**P-value**	**HR (95% CI)**	**P-value**
Unadjusted	1.406 (1.026 - 1.928)	0.03	2.523 (1.599 - 3.979)	<0.001
Adjusted for age, gender, Hr and FVC% pred. (key predictors)	1.769 (1.229 - 2.547)	0.002	1.825 (1.003 - 3.321)	0.05
Adjusting for other predictors (stepwise forward process) in a model with key predictors				
RVSP	1.100 (0.697 - 1.735)	0.68	2.163 (1.180 - 3.965)	0.01
PVRI	1.299 (0.832 - 2.028)	0.25	1.251 (0.641 - 2.441)	0.51
DLCO% pred.	1.947 (1.174 - 3.229)	0.01	1.625 (0.746 - 3.541)	0.22

PH-IPF: Pulmonary hypertension in IPF; mPAP: Mean pulmonary arterial pressure; RVSD: Right ventricular systolic dysfunction; SVI: Stroke volume index; CI: Conficence interval; PVR: Pulmonary vascular resistance; HR: Hazard ratio; Hr: Heart rate; FVC % pred.: Forced vital capacity % predicted; DLCO% predicted: Lung diffusion capacity for carbon monoxide % predicted; RVS: Right ventricular systolic pressure; PVRI: Pulmonary vascular resistance index.

2.3.5.2 Multivariable analysis

We adjusted the unadjusted dichotomous mPAP and SVI with key predictor variables age, gender, heart rates and FVC% predicted, selected based on literature reports [18]. The risk of mortality increased and remained significantly higher for PH in IPF subjects compared to IPF only subjects (HR: 1.769; 95% CI: 1.229-2.547, p= 0.002). Interestingly, the mortality risk remained significantly higher in subjects with RVSD compared to those with preserved RV function after adjusting for the key predictors (HR: 1.825; 95% CI: 1.003-3.321, p=0.049) (Table 3). Consistent with the unadjusted results, RVSD showed a stronger associated with mortality.

To assess the strength of the association between PH in IPF and RVSD, we performed logistic regressions with RVSD as the binary dependent variable and the mPAP as the dichotomized predictor variable. The likelihood of having RVSD was 3.38-fold (OR: 3.38; CI:

1.44-7.96; p=0.005) higher among those with elevated mPAP (>25mmHg) compared to those with normal pulmonary arterial pressures. Therefore, based on these findings, most patients with PH in IPF will eventually develop RVSD.

To determine the association between mPAP and SVI, RVSP, PVR, we performed pairwise Pearson's correlation tests. As expected, the correlation analysis between mPAP and SVI, showed a significant but mildly negative associated (r=-0.32, p=<0.001) (Figure 4). This indicates a worsening RV function as the mPAP (RV afterload) increases.

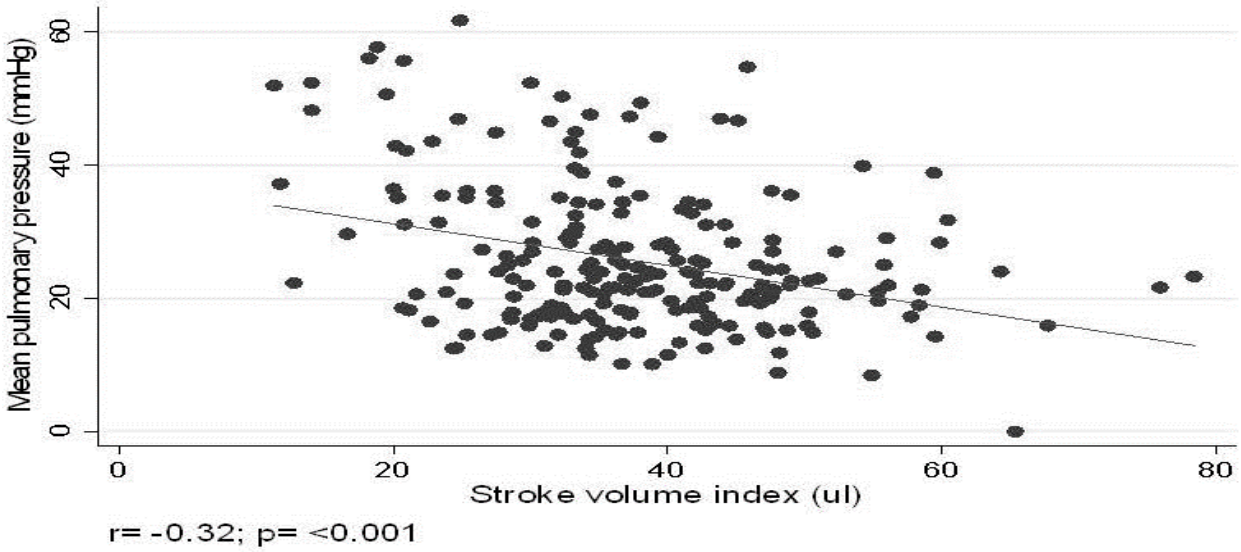

Figure 4 Correlation plot of mPAP vs SVI

There was also a strong correlation between mPAP and RVSP (r=92; p=<0.001) and between mPAP and PVR (r=0.75; p= <0.001). These variables, mPAP, RVSP and PVR are highly correlated, suggesting they are factors that measure the same underlying construct of a sick cardiopulmonary unit.

2.4 DISCUSSIONS

In this study, we found that the overall median survival was 3.7 years, and the 1-year and 5-year survival rates were 81.3% and 37.5%, respectively. There was a 43.8% decline in survival in five years following diagnosis. Indicating more than half of the IPF patents died in five years. In recent reports, IPF patients have been regrouped as slow (with several years of decline in lung function leading to death) and rapid progressors (less than six months of symptoms before their first presentation)[18]. The IPF patients in our cohort appeared to have a spectrum in their progression, leaning towards a slow progression pattern.

The Kaplan-Meier curves showed a significantly lower survival estimates in the PH-IPF patients when compared with IPF alone at one year (72.3 % vs 85.3%) and at five years (37.9% vs 49.6%). This suggest PH in IPF is associated with worse outcomes. Using RHC, Lettieri and colleagues in their evaluation of PH in IPF patients listed for lung transplantation found a one-year survival of 72% compared to 94.5% in IPF alone. This gives a difference in survival between the two groups of 22.5% compared to 13% in our cohort [79]. The higher difference in this study can be partly explained by the severity of the disease in a cohort made of patients listed for lung transplantation with advanced disease. Similarly, looking at patients with advanced lung disease awaiting lung transplant, Nathan and colleagues, performed serial RHC for PH in IPF at baseline (38.6%) and at the time of lung transplant (86.4%). They found that almost all the IPF patients developed PH late in the course of their disease [80]. The significant difference between these studies and ours is that their IPF cohort came from referral centers where IPF patients are listed for lung transplantation, whereas our cohort is from a regional registry that has IPF patients with a spectrum of disease severity, which is more indicative of the real-world picture.

Conversely, survival estimates of subjects with RVSD were significantly lower at one year (67.2% vs 83.7%) and at five years (16.8% vs 55.4%) compared to those without RVSD. Interestingly, these rates were lower among RVSD subjects compared with PH in IPF at one-and five-year by 5% and 21%, respectively. This indicates outcomes are markedly worse in IPF patients with associated RVSD than among those with PH in IPF.

In the multivariable Cox regression analysis, we found that the risk of mortality remained significantly higher for PH in IPF subjects compared to IPF alone (HR: 1.769; 95% CI: 1.229-2.537) after adjusting for key covariates (age, sex, heart rate and FVC % predicted). Interestingly, the mortality risk remained significantly higher in subjects with RVSD compared to those with preserved RV function after adjusting for the same key covariates (HR: 1.825; 95% CI: 1.003-3.321). More importantly, RVSD showed a stronger association with mortality than PH in IPF. There is very limited data with the use of RHC to evaluate the RV function in IPF. Nonetheless, Rivera-Lebron et al, studying 135 IPF patients referred for lung transplantation by transthoracic doppler echocardiography, found that RVD was associated with doubling of the risk of death. The authors used RV outflow tract velocity time integral (RVOT VTI), as a surrogate of stroke volume and the right atrial to left atrial ratio to assess RVD. They also reported an 11% prevalence of RSD in their cohort of IPF patients evaluated for lung transplantation [15].

Our correlation analyses revealed that the mPAP and SVI, showed a significant but mildly negative association (r=-0.32, p=<0.001). Furthermore, there was a strong correlation between mPAP and RVSP (r=92; p=<0.001) and between mPAP and PVR (r=75; p= <0.001). Interestingly, these variables (mPAP, RVSP, PVR) are all associated with the pulmonary vascular load or afterload. Several publications have reported that outcome in PH is more related

with the capacity of the RV to adapt to elevated afterload [5, 25]. Recently, Corte et al, performed RHC on 66 patients with diffuse interstitial lung disease and showed that PVR was an independent predictor of mortality (OR, 1.3, P= <0.001) [81].

Also, the results from this study showed that both PH and RSVD are prevalent in IPF. The prevalence of PH in IPF was 28.6%. Lettieri and colleagues reported a 31.6% [79] and Shorr et al reported a 46.1% [82] prevalence of PH in IPF. These prevalence rates may have been overestimated since these studies were performed before the 2008 Dana Point conference on pulmonary hypertension that set two hemodynamic cutoff points (mPAP≥25mmHg and PCWP ≤15mmHg at rest by RHC), for the diagnosis of pulmonary hypertension [12]. Moreover, these studies were conducted in referral centers on the records of IPF patients listed for transplant with advanced disease.

The prevalence of PH in IPF has also been evaluated from registries with a wide range of estimates. Lederer and collaborators found that 36% of IPF patients from the US United Networks for Organ Sharing (UNOS) database had PH in IPF [83]. In a recent publication from the UNOS registry, Hayes and colleagues reported a 49% prevalence of PH in IPF following lung transplantation [84]. Together, these studies indicate that PH in IPF is common and adversely affect outcomes. However, none of these studies assessed the impact of the right ventricular function on outcomes.

Our results showed that 12.3% of the IPF patients in our cohort had RVSD. These findings are consistent with that of Rivera-Lebron and colleagues who assesses echocardiographic predictors of mortality in a cohort of IPF patients referred for lung transplantation. They found that in this cohort, the prevalence of moderate to severe RVD was

11% and an independent predictor of mortality measured by the ratio of the right atrial to left atrial diameter and RVOT VTI [15].

Limitations. Our study has some limitations, such as the retrospective review from a single center registry. Though the data was from a single center, the Simmons Center for ILDs is a regional and member of PA-state wide IPF registry with subjects presenting with diverse disease severity spectrum and different demographic backgrounds. The diagnosis of IPF is ultimately one of exclusion, fact that some of the diagnosis of IPF were made before the 2002 ATS/ERS criteria for diagnosing IPF. These probably lead to the misdiagnosis of some IPF subjects. Also, the threshold levels in our analysis were predefined based on existing literature for both RVSD and PH in IPF. It is, however, possible that different threshold values might have yielded different results. We did not include in our analysis the different medications that the IPF patients were taking that might affect survival. Notwithstanding these limitations, the strength of our study is in the use of data generated by the gold standard RHC, in a registry with real-world characteristics to assess the RV function in an IPF-specific population.

3.0 THE THERAPEUTIC POTENTIAL OF MSC-DERIVED EXOSOMES IN FIBROTIC LUNG INJURY

3.1 INTRODUCTION

There is no effective treatment for IPF except for lung transplantation. The recently approved antifibrotic/anti-inflammatory medication, pirfenidone and the tyrosine kinase inhibitor, nintedanib, only help slow disease progression. Consequently, there is an urgent need for novel therapeutic approaches in IPF. It has been argued that IPF is a non-inflammatory condition because it is refractory to corticotherapy [1, 85]. However, this theory overlooked the role played by immune cells in the wound-healing process that has been demonstrated in the pathogenesis of IPF[86]. This suggest that agents with anti-inflammatory properties can be effective therapies in IPF. Although the pathogenesis of IPF is not fully elucidated, its histopathologic pattern of usual interstitial pneumonia (UIP) is well known. UIP is characterized by areas of fibroblast/myofibroblast proliferation, deposition of extracellular matrix (ECM) and collagen, referred to as the fibroblastic foci, interspaced with normal lung tissue. This pattern suggests a progressive fibroproliferative process [85]. Put together, novel therapeutic agents that demonstrate pleiotropic anti-inflammatory, antifibrotic and immunomodulatory effects hold promise as potential therapeutic options for IPF. There is growing evidence that indicates hMSCs and their derived exosomes possess these triple (antifibrotic, anti-inflammatory and immunomodulatory)

ameliorating effects in fibrotic lung disease[6, 33]. More importantly, hMSC exosomes have greater appeal as therapy for IPF than their parent MSCs because they are believed to be less toxic with a lower risk to immunologic rejection following allogeneic infusions[52]. Furthermore, hMSC-derived exosomes have membranes that protect their macromolecular cargo and facilitate their storage and scalability. Also, there is a lower risk of inducing changes in chromosome numbers (aneuploidy), which is feasible with whole MSC infusions. Interestingly, exosomes are reported to have immune-privileged properties just as their parent cells with fewer ethical implications [52, 53]. These posited immune-privilege properties of hMSC exosomes make them prime candidates for therapy in fibrotic lung disease-induced RVD. However, there is limited data on the modulatory effects of hMSC exosomes on the RV function within the context of FLI-induced pulmonary vascular overload. Therefore, it will be biologically relevant to assess the modulatory effects of hMSCs and their derived exosomes on the RV function in a mouse model of FLI.

Right heart catheterization (RHC) and PV loop analysis remain the gold standard for defining changes in PH and assessing the hemodynamic load on the RV [4]. Nonetheless, it is important for PV loop analysis to be performed appropriately by skilled personnel and for the results to be reliable and accurate. In unskilled hands, measuring ventricular volumes using PV loop analysis can be very challenging. This is because volumes are estimated from the conductance of an electric field, generated by miniaturized electrodes in the catheters, which passes through blood and the myocardium. To calculate the absolute ventricular volume, the contribution of the myocardium to conductance (parallel conductance) has to be removed from the total conductance [87]. To this end, two catheter-derived PV loop technologies are available; the traditional conductance catheter that requires in vivo calibration using a bolus of hypertonic saline to estimate the parallel conductance, and the new admittance catheter that instantaneously

corrects for the parallel conductance [88]. In this study, we used the admittance catheter system because of its capability to generate instantaneous absolute volumes without the perilous in vivo calibrations linked with the conductance catheters. PV loop analysis with admittance catheters have the unique ability to evaluate PH, RV afterload, their interactions and gauge the response of the cardiopulmonary unit to novel therapeutics, including hMSC exosomes [4, 24]. Importantly, PV loop analysis can assess the RV adaptation to the increased RV afterload [26]. When these adaptive compensatory mechanisms are surmounted by the increasing pulmonary pressure overload, RVD ensues and progressively lead to uncoupling (RV failure) of the RV from the pulmonary vasculature. To highlight these compensatory changes, Kubba S. et al, reported that RV-PA coupling is a preserved when there is an adaptive increase in contractility (onset of RVD) to match increased RV afterload [25]. This indicates that in compensated RVD, there is RV-PA coupling. Uncoupling ensues when RV contractility is not increased to overcome RV afterload, which correlates with pulmonary vascular resistance (PVR). There is therefore, a progressive transition to a decompensated RVD with uncoupling and overt RV failure. This interaction between the RV and pulmonary vasculature supports the notion of studying the RV and the pulmonary vasculature as an integral functional cardiopulmonary unit [51, 89].

The RV contractility reserve is reported to be 5-fold higher than that of the LV, giving it a relatively longer period to adapt to the increased pulmonary vascular load before the onset of a decompensated RV failure [10]. Spruijt et al, tested this concept of reactive contractility increase in patients with IPAH and showed that they already had maximally increased RV contractility at rest, indicating an early onset of RVD [26]. Consequently, assessing indices of RV contractility using PV loop analysis can provide insights into the onset RVD [51, 89, 90]. We therefore, sought to employ RHC and PV loop analysis to evaluate the RV adaptation to increased pulmonary

pressures associated with FLI, and assess their response to hMSC exosome treatment. We hypothesized that hMSCs exosomes exert their beneficial effects in part, by modulating RV contractility.

3.2 MATERIALS AND METHODS

3.2.1 Design

This study was an in vivo experimental design aimed at recapitulating human IPF in a mouse model of bleomycin-induced fibrotic lung injury. Pressure-volume (P-V) loop analyses were performed to assess the RV function after fibrotic lung injury followed by transplantation of exogenous hMSCs and their derived exosomes. All animal protocols were approved by the University of Pittsburgh Institutional Animal Care and Use Committee (IACAUC).

3.2.2 Isolation and Characterization of human MSC-derived exosomes

Clinical grade bone marrow-derived hMSCs were obtained from the NHLBI-sponsored Production Assistance for Cellular Therapies (PACT) program based at the University of Minnesota, MN [91]. Exosomes (EXO-20) were isolated from these hMSCs as previously described by our group and others [45, 92]. Briefly, hMSCs were cultured and expanded in T175 cm^2 flasks (ThermoFisher Scientific) to 80% confluency for the first passage, and then separated into three T175 flasks for the second passage to 80% confluency. Thereafter, the cells from three T175 flasks (on average $20*10^6$ cells) were washed, detached, and seeded in a triple-layer flask

(ThermoFisher Scientific) with 400ml of exosome-depleted maintenance media. Every other 48 hours, the conditioned media was collected and passed through multiple differential centrifugation (300g/10mins, 2000g/20mins, 10,000g /hour) followed by an ultracentrifugation step on a sucrose cushion (100,000g/2hours) [93].This process was repeated to have 8-10 collections/isolates of exosomes from the same parent hMSC that was pooled for protein assay using a Micro BCA^{TM}Protein assay kit (ThermoFisher Scientific) and their size distribution/concentrations were evaluated by Nanosight Tracking Analysis on a NanoSight LM10 (Malvern, Westborough, MA).

3.2.3 Mouse model of bleomycin-induced fibrotic lung injury

Ten-12-weeks old female C57BL/6N mice (Charles River Laboratories, Wilmington, MA) were randomly assigned, to four experimental groups/conditions (Controls, bleomycin (BLM) only, BLM+hMSC, BLM+exosome]. Ear tag numbers were used to generate random numbers that were randomly assigned to the four experimental conditions. To induce fibrotic lung injury, twelve doses of 20U/kg of bleomycin (APP Pharmaceuticals, Schaumburg, IL) were administered subcutaneously in 100ul of normal saline every other day for a total of 240U/kg [29, 94]. Following established lung injury after the sixth dose of BLM, the first dose of 500,000 human mesenchymal stem cells (25 x 10^6 MSCs/kg, body weight) and exosomes (50ug/kg, body weight) were injected intravenously by the jugular vein in 160ul of normal saline-vehicle. The control mice received the same volume of vehicle. A second dose of the same amount of hMSCs or exosomes was given intravenously by tail vein after the twelfth injection of BLM. The mice were monitored and anesthetized for PV loop analysis 7 days after the last dose of BLM for a total exposure period of 31 days.

3.2.4 Animal handling and pressure-volume loop measurements

The mice were anesthetized with intraperitoneal urethane (ethyl carbamate) solution (1 mg/g, body weight) and intubated with a 1.3 mm cannula. The cannula was connected to a ventilator that was set at a tidal volume of 225ul with 200 breaths/min. An apical stab wound was established with a 20G needle to insert a 1.2 F admittance pressure-volume catheter (Transonic Systems Inc, Ithaca, NY) into the RV (Figure 1). The admittance catheter has features to instantly measure pressures and simultaneously determine absolute volumes by calibrating phase shifts of the generated electrical fields. These phase shifts are used to subtract the contribution of the ventricular wall (parallel conductance) to the overall volume signal [95, 96]. After setting the instruments, PV loop analysis were performed at steady state and following caudal vena cava occlusion for load-dependent and load-independent values, respectively. The right ventricular pressure and volume readings were captured on an ADV500/ ADVantage system (Transonic Systems Inc, Ithaca, NY) with an integrated LabChart software (ADInstruments Inc., Colorado Springs, CO) for post-data acquisition analysis. [97].

3.2.5 Pressure-volume loop analysis

The P-V loops used in our analysis went through a quality control process by the P-V loop data analyst. For each experimental condition, at least 10 consecutive cardiac cycles free of arrhythmias were selected and recorded for further analysis. The selection was done consistently across the experimental dataset with and without caudal vena cava occlusion. Standard hemodynamic variables (heart rate, systolic and diastolic pressures), right ventricular function volumetric parameters (CO, EF, SV), Ees, and Ea were recorded from the hemodynamic data

(Table 4). Contractility was quantified from the slopes of the ESPVR (Ees), PRSW, and the dP/dt_{mx}-end diastolic volume (dP/dt_{mx}-EDV) relationships. Finally, right ventricular-vascular coupling efficiency was calculated as Ees/Ea ratio [70, 96, 98].

3.2.6 Primary and secondary outcomes

Our primary endpoint was RV contractility that was determine from the slopes of three indices (ESPVR (Ees), PRSW, and dP/dt_{mx}-EDV relationship. The secondary endpoints were right ventricular systolic pressure, mean pulmonary arterial pressure (mPAP), pulmonary vascular resistance (PVR) and the right ventricular elastance-to-pulmonary artery elastance (Ees/Ea) ratio.

3.2.7 Sample size and power calculations

The level of significance (α) and power ($1-\beta$) were set a priori at 0.05 and 0.8, respectively. The power to detect a 0.5 change in the slope of the ESPVR (Ees) and its standard deviation (0.20), were obtained from the first study ever reported on the RV function in mice using P-V loop analysis [97]. A G*Power statistical package [99] with its integrated ANOVA F-test, was used to determine a minimal sample size of 55 mice needed to detect a 0.5 change in the end-systolic elastance between the experimental conditions.

3.2.8 Statistical analysis

The data were summarized as the mean±SEM or median where appropriate, and dot plots to show the raw data. An ANOVA or a Kruskal–Wallis tests were used for three or more group

comparisons. Where necessary, a Tukey-Kramer or Dunn post-hoc multiple comparison tests were performed when the overall F-test was significant. A p-value of <0.05 was the statistically significant threshold and STATA statistical software (StataCorp, College Station, TX, Version 15.0) was used for all analyses. The non-parametric Kruskal-Wallis test was used when the ANOVA assumptions were not met.

3.3 RESULTS.

Our findings showed that the average body weight of the BLM injured group was significantly lower when compared to controls ($p < 0.05$; 18.0 ± 0.33 vs 22.2 ± 0.40, g). The weight loss was significantly increased by administering human MSCs (18.0 ± 0.33 vs 21.5 ± 0.60, g) and EXO-20 (18.0 ± 0.33 vs 20.1 ± 0.49, g). This indicated a beneficial effect on weight gain following the injection of both hMSCs and exosomes (Table 4).

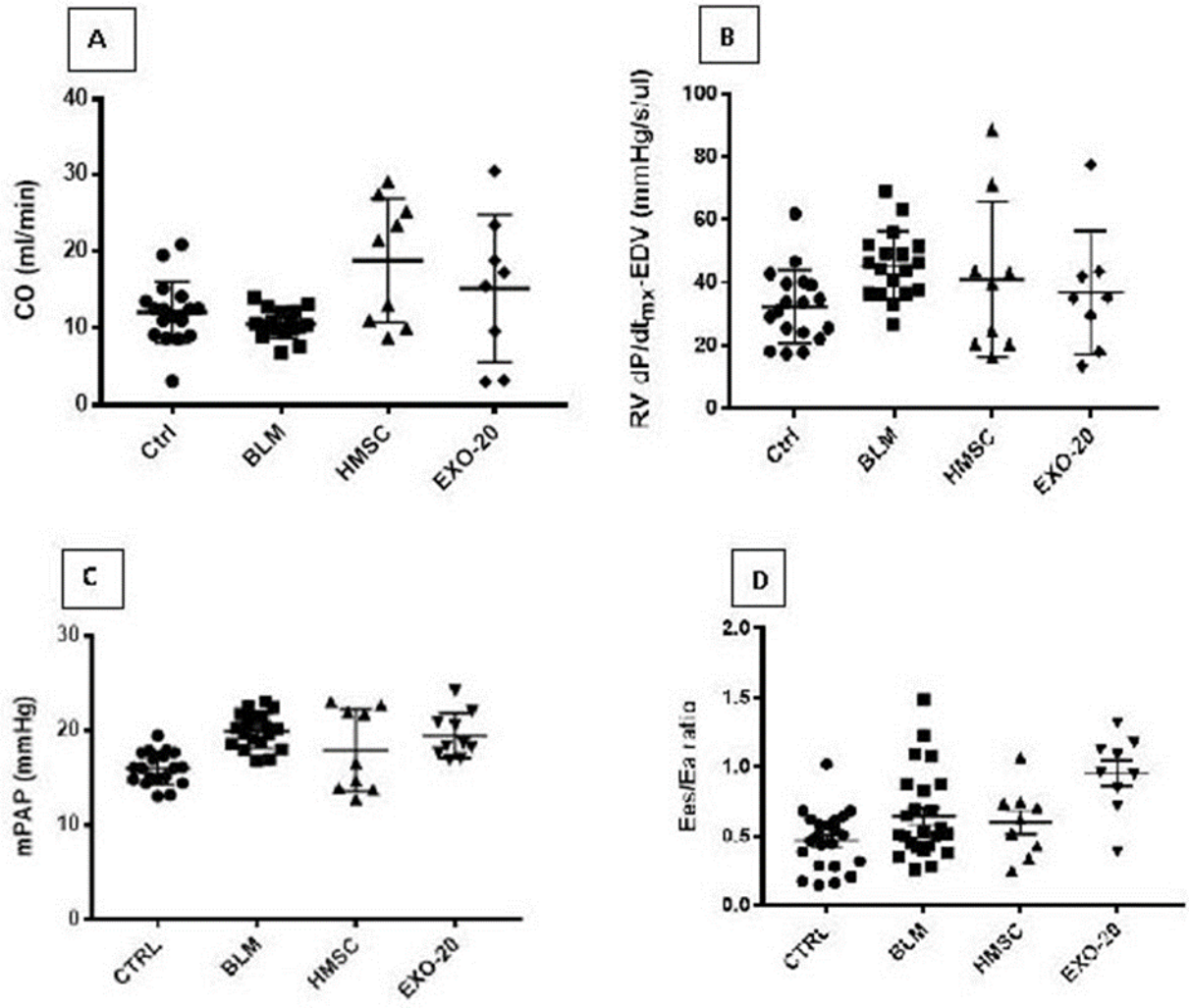

Figure 5 Dot plots: Indices of RV contractility (A & B), afterload (C) and coupling efficiency (D).

3.3.1 Cardiopulmonary hemodynamic data.

Load-dependent measures of contractility (EF, SV) were slightly lowered by BLM injury (47 vs 48, %; 21.6± 0.88 vs 23.8±1.57, ul), respectively. Moreover, BLM injury significantly reduced the CO (10.5±0.43 vs 12.2±0.98, ml/min), which is another index of load-dependent contractility, from baseline-controls (Figure 5). This reduction was significantly increased by

injecting hMSCs (18.8±2.69 vs 10.5±0.43, ml/min) and exosomes (17.2±2.59 vs 10.5±0.43, ml/min).

Table 4 Hemodynamic characteristics and indices of pressure-volume relationships

	CTRL	BLM	HMSC	EXO-20	Significant pairwise comparisons (p<0.05)
Paramaters					
BW, *g*	22.2 ± 0.40	18.0 ± 0.33	21.5 ± 0.60	20.1 ± 0.49	CTRL vs BLM; BLM vs HMSC; BLM vs EXO-20$^{\phi}$
BSA, cm^2	77.7 ± 0.94	67.6 ± 0.82	75.9 ± 1.43	72.6 ± 1.18	CTRL vs HMSC; BLM vs HMSC$^{\phi}$
mPAP, *mmHg*	16.1 ± 0.43	20.0 ± 0.45	17.8 ± 1.45	19.4 ± 0.76	CTRL vs BLM; CTRL vs EXO-20‡
Heart rate, *beats/min*	506.4 ± 15.17	490.0 ± 13.34	583.2 ± 21.39	516.9 ± 16.46	CTRL vs HMSC; BLM vs HMSC$^{\phi}$
RV-systolic pressure, *mmHg*	23.9 ± 0.66	29.8 ± 0.69	26.6 ± 2.24	29.0 ± 1.16	CTRL vs BLM; CTRL vs EXO-20‡
RV-diastolic pressure, *mmHg*	0.89 ± 0.08	1.15 ± 0.08	1.50 ± 0.47	1.06 ± 0.12	None
End-diastolic volume, *ul*	49.4 ± 2.25	46.4 ± 1.80	67.4 ± 10.13	64.0 ± 9.49	None
Stroke volume, *ul*	23.8 ± 1.57	21.6 ± 0.88	32.5 ± 4.56	33.1 ± 5.26	None
Stroke work, *mmHg.ul*	364.4 ± 28.90	406.9 ± 20.10	492.0 ± 62.16	686.9 ± 169.25	None
Cardiac output, *ml/min*	12.2 ± 0.98	10.5 ± 0.43	18.8 ± 2.69	17.2± 2.59	BLM vs HMSC; BLM vs EXO-20‡
Systolic indices					
Ejection faction, *%*	48.3 ± 2.53	47.2 ± 1.93	49.0 ± 3.41	55.0 ± 6.23	None
$dP/dt_{max.}$, *mmHg/s*	1526.5 ± 83.12	2043.9 ± 56.76	2199.1 ± 148.61	1890.7 ± 67.79	CTRL vs BLM/HMSC/EXO-20$^{\phi}$
$dP/dt_{max.}$- end-diastolic volume, *mmHg/s/ul*	32.8 ± 2.87	45.5 ± 2.52	41.0 ± 8.26	36.1 ± 6.13	CTRL vs BLM‡
Ees, *mmHg/ul*	0.55 ± 0.09	0.72 ± 0.06	0.56 ± 0.09	0.81 ± 0.09	None
PRSW, *mmHg*	7.4 ± 0.50	8.9 ± 0.47	7.8 ± 0.91	10.3 ± 1.33	None
Pulmonary vascular indices					
Ea, *mmHg*	1.1 ± 0.12	1.4 ± 0.07	1.0 ± 0.22	1.7 ± 0.56	CTRL vs BLM‡
PVR, *wu*	1.2 ± 0.07	1.7 ± 0.08	1.1 ± 0.20	1.2± 0.41	CTRL vs BLM; BLM vs HMSC; BLM vs EXO-20‡
Coupling efficiency					
Ees/Ea	0.53 ± 0.05	0.51 ± 0.04	0.60 ± 0.08	0.96 ± 0.29	None

Values are means ± SEM; n= 9 to 18 per group; BW: Body weight; BSA: Body surface area (Meeh's formula); mPAP: Mean pulmonary arterial pressure; dP/d_{max}: Maximum ventricular pressure derivative; Ees: Ventricular end-systolic elastance; Ea: Effective arterial elastance; PRSW: Preload recruitable stroke work; PVR: Pulmonary vascular resistance; wu: Wood unit.; P< 0.05 by $^{\phi}$Tukey-Kramer's and ‡Dunn's multiple comparison tests following an overall significant oneway ANOVA and Kruskal Wallis analyses, respectively.

3.3.2 Afterload

Indices assessing RV afterload (mPAP, RVSP, PVR) showed a wide range in their response to an intervention with hMSCs and exosomes. As shown in Table 4, the mean pulmonary arterial pressure (mPAP) was significantly increased in the BLM injury group when compared with controls (20.0±0.45 vs 16.1±0.43, mmHg). The BLM-induced increase in pulmonary pressure was attenuated but insignificantly after administering hMSCs and exosomes. The same trend was observed in the RV systolic pressure (RVSP) when comparing the BLM injury group with controls (29.8±0.69 vs 23.9±0.66, mmHg) and following injections of hMSCs and exosomes (Table 4). However, the pulmonary vascular resistance (PVR), another metric of afterload, was significantly increased by BLM injury when compared with controls (1.7±0.08 vs 1.2±0.07, wood unit). The injection of hMSCs and exosomes significantly reduced the BLM-induced increase in afterload (1.7±0.08 vs 1.1±0.20; 1.7±0.08 vs 1.2±0.41, wood), respectively. Collectively, both hMSCs and exosomes had beneficial, but mostly nonsignificant, effects in reducing the RV afterload. This data indicates that the beneficial effects of hMSCs and exosomes on RV afterload in this study might have been insufficient because of its dose-dependent effect.

3.3.3 Contractility

All three load-independent measures of contractility, Ees, PRSW, and dP/dt-EDV increased but not significantly after BLM injury compared with controls by 24%, 17%, and 28%, respectively. However, only the increase in contractility comparing dP/dt_EDV in the BLM injury group with controls was statistically significant (45.5±2.52 vs 32.8±2.87, $mmHg.s^{-1}. ul^{-1}$). There was a marked but nonsignificant reduction in contractility following treatment with both hMSCs and

exosomes (Table 4). Similarly, as noted above with afterload, this suggested a potential dose-dependent effect of hMSCs and exosomes on RV contractility. The P-V loops in Figure 6 illustrate the changes in contractility under the different experimental conditions. The greater the steepness of the slope of the end-systolic pressure to volume relationship (ESPVR), the stronger the contractility. There is a stronger and possibly complete RV contraction when comparing the BLM group to controls (Figure 6). The contractility in the hMSC group was reversed towards that of the controls, indicating an improvement in RV contractile reserve.

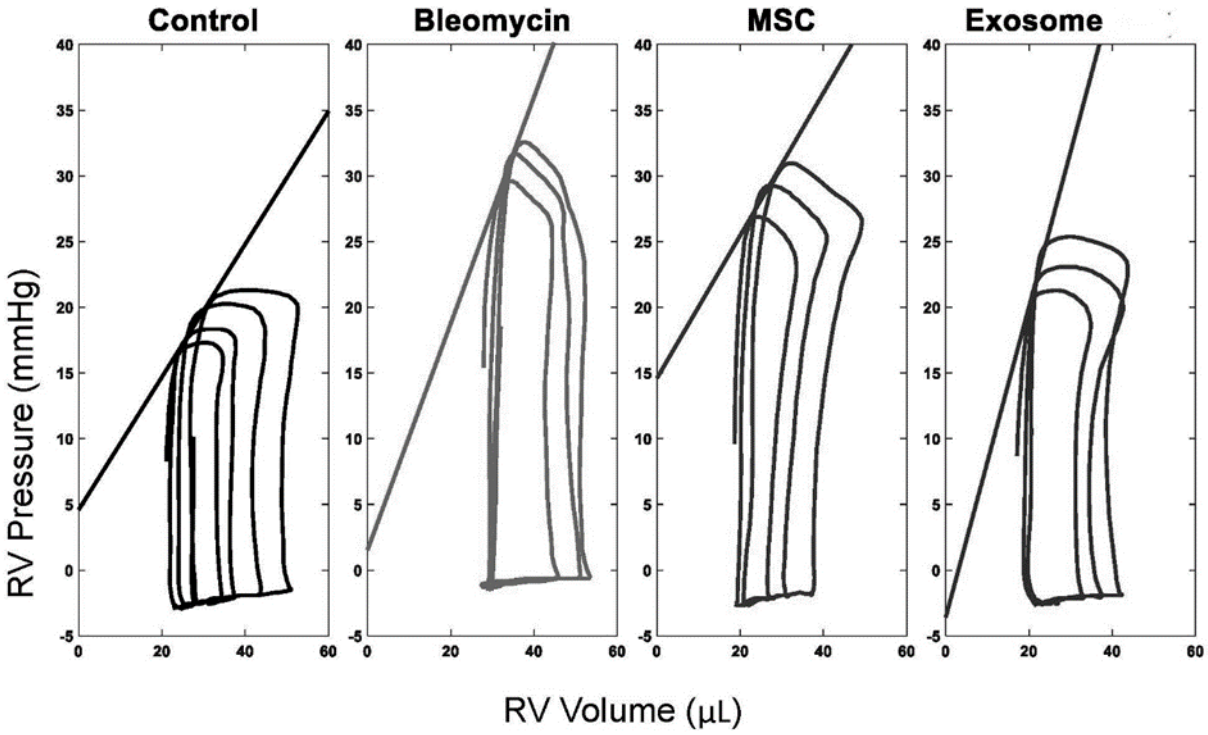

Figure 6 Slopes of the end-systolic pressure-volume relationships

3.3.4 Coupling efficiency

The coupling efficiency, which is the optimal RV work to pump blood through the pulmonary artery with minimal energy consumption, is assessed by the Ees/Ea ratio. It showed a nonsignificant decrease comparing BLM injury to control groups (0.51 vs 0.53). There was a minor beneficial effect from injury after administering hMSCs and exosomes (Table 4 & Figure 5). Overall, the coupling efficiency was determined to be suboptimal since all the ratios were above 0.5. This indicated that the coupling efficiency of the RV supply to the pulmonary vasculature demands was maintained despite the BLM-induced increase in the RV afterload.

3.4 DISCUSSIONS

The results showed that the RV afterload was significantly increased and accompanied by an adaptive increase in RV contractility from baseline. Furthermore, the intravenous injections of hMSCs and exosomes after an established fibrotic lung injury, showed beneficial effects on right ventricular contractility and afterload. Some of the insignificant beneficial effects could have been in part, due to the dose-dependent mode of action of both hMSCs and exosomes.

Afterload. We found that BLM injury significantly increased RV afterload indices (RVSP, mPAP, PVR) that were reversed by hMSCs treatment. Similarly, lower improvements were observed after treatment with exosomes (Table 4). Consistent with our results, Tabima D. et al [97] using admittance-derived PV loop analysis, also found a significant (67.5%) increase in RVSP from controls following hypoxia-induced pulmonary hypertension (45±17 vs 27±3,

mmHg) [97]. Evaluating sixty-six patients with diffuse parenchymal lung disease, Corte T et al found an elevated PVR (≥ 6.23 WU) as the strongest hemodynamic predictor of mortality, but RVSP and mPAP were not predictive of mortality [81]. Even though these reports showed mixed findings relating RVSP and mPAP to outcomes, they all provide support for PVR as a strong predictor of mortality.

Contractility. The RV supply (contractility) of blood flow assessed by a load-independent index of contractility ($dP/dt_{max.}$-EDV), was significantly higher among the BLM injury group when compared with controls. An adaptive increase in contractility has been reported as an early sign of RVSD [90]. Recently, Guihaire et al and others, showed that an increased pulmonary hypertension was associated with a reduction in contractile reserve during exercise [26, 100, 101]. These authors argue that subjects with PH already have maximally increased RV contractility at rest that could not adapt to the increased afterload during exercise. In our bleomycin model of fibrotic lung injury (FLI), we found a 28% increase in RV contractility (an early sign of adaptive RVSD), using the slope of the maximum pressure derivative to the end diastolic volume (dP/dt_{max}-EDV). This increase in contractility was attenuated by administering hMSCs and exosomes (Table 4). The increase in RV contractility as an early sign of RVD has been reported by other investigators in human subjects and animal models [26, 101]. Tabima D. and colleagues, in a mouse model of hypoxia-induced pulmonary hypertension, found a 110% increase in contractility based on evaluating the dP/dt_{max}-EDV relationship [97]. Yerebakan C. et al studying the RV adaptation to increased pressure overload in sheep, found a significant increase in RV contractility based on an increase in the maximal slope of systolic pressure increment (dP/dt_{mx}, $p=0.002$)[101]. Most recently, Spruijt et al evaluating patients with precapillary PH, determined that failure to compensate for the further increases in pulmonary pressure during exercise, led to

a poor RV contractility matching the increased RV pressure overload [26]. Collectively, therefore, an increase in RV contractility is an early indicator of RVD. Of the indices routinely used to assess RV contractility (Ees, PRSW, dP/dt_{max}-EDV), dP/dt_{max}-EDV was reported as the most reliable load-independent measure of contractility [97] and thus, confirming our use of this index as a measure of RV contractility.

Coupling efficiency. The ratio of ventricular elastance (Ees) to the effective arterial elastance (Ea), provides a quantitative assessment of how the RV ventricular systolic function adapts to increased RV afterload [22]. In mice, a ratio greater than 0.5 shows that the ventricle is operating at optimal efficiency with minimal energy spent to overcome the RV afterload [102]. Our findings showed an Ees/Ea ratio that was borderline greater than 0.5 in all experimental conditions. This suggest a preserved, suboptimal ventricular-arterial coupling efficiency and a state of compensated RVD. Wauthy et al, studying RV contractile function in different large animal species (dogs, goats, pigs), also reported a preserved optimal ventricular-arterial coupling despite an increase in pulmonary hypertension [27]. Put together, a preserved ventricular to pulmonary vascular coupling does not preclude an underlying RVD because is reflection of an interaction between RV contractility (Ees) and RV afterload (Ea).

Notwithstanding the potential beneficial effects of hMSC and their exosomes in fibrotic lung injury and cardiac remodeling, the contributions of resident tissue stem cells in the heart and lungs is still not fully understood [37, 103].It was recently reported that resident tissue MSCs may differentiate in a hierarchical fashion with increased specificity in tissue repair function according to the paracrine and autocrine cues in their microenvironment [104]. A potential paracrine cue may come from the secreted exosomes of ex vivo transplanted hMSCs. Allogeneic hMSCs have been shown to ameliorate their bioenergetic properties by extruding mitochondria

to recipient cells through secreted extracellular vesicles [45, 105]. Therefore, mitochondrial transfer between transplanted hMSC exosomes and resident cardiac and lung stem cells will be a potential mechanism through which stem cells (endogenous and exogenous) interact to repair damaged tissues.

Limitations. In inexperienced hands, measuring cardiac volumes using an admittance catheter in mice is always challenging due to the crescentic trapezoid shape of the right ventricle [96]. We employed the expertise of the personnel at the Vascular Medicine Institute at the University of Pittsburgh who have gained much experience in conducting PV loop analysis in mice over the years. The volumes from our P-V loop data were relatively higher than those previously reported in mice [97]. This may have reduced the absolute values of some of the variables indexed by volume such as the $dP/dt_{max.}$-EDV, thus hindering effective comparisons with other studies. Despite this limitation, the trend and directions of our findings were comparable to previously published data. We did not use a dose escalation protocol for hMSCs and exosomes, which could have allowed us to draw clear conclusions on their dose-dependent effects.

4.0 A DESCCRIPTIVE PROTEOMIC ANALYSIS OF HMSC EXOSOMES: THERAPEUTIC IMPLICATIONS IN FIBROTIC LUNG DISEASES

4.1 INTRODUCTION

Human bone marrow-derived mesenchymal stem cells (hMSCs), which is the most studied of all hMSCs, hold promise as therapy for complex diseases such as fibrotic lung diseases [106, 107]. There has been a shift in paradigm, from the previous postulate that transplanted MSCs engraft and differentiation into damaged resident cells to one based on MSCs releasing paracrine effectors[52]. The hMSC secreted paracrine factors (secretome) comprise soluble factors and insoluble extracellular vesicles (EVs)[33]. These EVs include nanosize exosomes (30-100 nm in diameter), which originate from the endosomal compartment, and microvesicles (MVs, 0.1 to 1μm in diameter), which are formed from plasma membrane blebs [108]. While MVs can be isolated from biofluids and cell culture supernatant at low centrifugation (10,000-12,000g), the isolation of exosomes requires ultracentrifugation at 100,000-120,000g [109].

Human MSC exosomes have been demonstrated to protect mice from myocardial infarction, pulmonary arterial hypertension and bleomycin induced fibrotic lung disease [56, 110]. Also, their use in clinical trials have been reported in other countries [39]. Despite the excitement generated in the potential of hMSC exosomes to treat fibrotic lung diseases, however, the components of the hMSC exosome proteome that is responsible for their therapeutic effect are

still not well characterized. Identifying the unique protein components that confer the therapeutic effects of hMSCs will go a long way in filling the current knowledge gap in markers of hMSC therapeutic efficacy/potency. Biomarkers of MSC potency or efficacy are key to translating hMSC exosomes into reproducible and measurable clinical applications. Lee RH. and colleagues recently reported the expression of TSG6 as a biomarker to predict the efficacy of BM-MSCs prepared by standardized protocols. Surprisingly, they found that only one-third of their preparations expressing high levels of TSG6 produced beneficial effects in a mouse model of induced inflammatory cornea disease [40]. Other investigators have suggested Twist 1 as predictive biomarkers of the proliferative potential of hMSCs. They correlated high proliferative capacity with therapeutic potency based on in vitro assays [111]. Put together, adequate candidate biomarkers that are predictive of hMSC efficacy need to be identified and validated, in vivo in animal models. The assumption is that efficacious hMSCs will also release efficacious exosomes, but several studies have shown that exosomes are differentially enriched in miRs and mRNAs and potentially their protein load when compared with their parent cells [49]. Therefore, protein components that can be identified and validated as adequate biomarkers directly from exosomes will be better predictors of hMSC efficacy.

Recently, we showed that hMSCs exert their beneficial actions in part, by shuttling their extravesicular cargo (microRNA, proteins) to macrophages and, as a result, changed their immunomodulatory phenotype [45]. This study and others [53] suggest a potential cross-talk between hMSC exosomes and target cells such as endothelial, cardiomyocytes, and lung epithelial cells for tissue repair following different types of injury. In recent years, the role of oxidative stress in tissue injury, including fibrotic lung disease, has caught the attention of several investigators [57, 61]. Most reports have shown an increased expression of NADPH oxidase (NOX) and

mitochondria as the main sources of ROS production that led to the development of pulmonary and RV remodeling [59, 60]. These data suggest that excessive ROS production (oxidative stress) is deleterious to the normal interaction (coupling) of the RV to the pulmonary artery. Also, increased ROS generation has been shown to positively correlate with high levels of misfolded or damaged proteins [64, 65]. If allowed to accumulate and not degraded by homeostatic pathways, these misfolded proteins will invariably induce the injury observed in cardiopulmonary remodeling [59]. A key pathway in protein homeostasis is the ubiquitin/proteasome pathway [66, 112]. Proteasomes are an essential group of hydrolase proteolytic enzymes that have also been identified in exosomes [66]. According to these authors, proteasomes played a key role in clearing misfolded proteins to mitigate ischemia/ reperfusion (I/R) injury. Put together, these data indicate a pivotal role of proteasomes in the clearance of damaged proteins within cells. Their intracellular proteolytic effects may be augmented by the extracellular proteolytic effects of matrix metalloproteinases (MMPs) within the ECM. Specifically, the gelatinases (MMP2 and MMP9) are MMPs that play a critical role in ECM protein turnover [67]. Therefore, a combined antioxidant and proteolytic turnover of damaged proteins may in part, explain the pleiotropic beneficial paracrine effects of hMSC-based therapies reported in complex fibrotic lung diseases such as IPF. To facilitate the translation of hMSc exosomes from preclinical to clinical trials, the protein components that confer their therapeutic potential must initially be identified using modalities that can reliably analyze their complex protein cargo (proteomics) within a short timeframe. This has been made possible since the mid-90s with the development of high-performance liquid chromatography (HPLC) coupled to mass spectrometry (MS). The basic principles in proteomic analysis by MS initially involve loading microliters of a trypsin digested protein onto HPLC C (carbon)-18 columns. Analytes in solution are separated based on their

hydrophobicity and the eluted peptides are then transferred onto an electrospray ionization (ESI) device that is linked to a MS [113]. The peptides are ionized and fragmented to generate tandem mass spectrometry (MS/MS) spectra that are searched against curated protein databases for protein identification. Proteomic analysis of various complex protein cargos generates huge high-throughput data that need bioinformatic expertise and software for their analysis and further classification.

One of the first publications on the proteome of the hMSC exosome was from Lai R. and colleagues in the Lim S. laboratory in Singapore. They used proteomic analysis to demonstrate that the predominant component of the hMSC exosome proteome was the 20S proteasome. The 20S proteasome constitutes the catalytic core of the 26S proteasome that has been shown to have critical physiological and pathological implications in many diseases, including myocardial infarction and fibrotic lung diseases [65]. Furthermore, Lai R. et al showed that the presence of 20S proteasome correlated with a significant reduction in extracellular oligomerized or folded proteins, thereby, prompting these investigators to postulate that 20S proteasome may synergize with other components of the hMSC exosome proteome to ameliorate tissue injury [66]. Following this article, a proteomic analysis was conducted on hMSC-derived MVs to investigate their therapeutic cargo by Kim H. et al. These authors reported that the proteome of hMSC MVs was enriched in cell surface receptors, cell adhesion and signaling molecules that may be associated with their beneficiary effects [114]. Put together, the findings of these early proteomic analysis of the hMSC exosome proteome, support the notion that hMSCs mediate their paracrine effects via exosomes that carry proteins with cell signaling and proteolytic properties. Most recently, Anderson J. et al, conducted a quantitative proteomic analysis of BM-MSC exosomes that revealed they possess modulatory properties in angiogenesis. These investigators further

demonstrated that the proteome of hMSC exosomes cultured under reduced oxygen, peripheral arterial disease-like, conditions (serum starved with a 1% oxygen tension) contained an enriched profile of angiogenic signaling proteins that induced angiogenesis via the nuclear factor kappa-light chain enhancer of activated B-cells (NFkB) pathway [115]. Similarly, Haraszti RA and colleagues in their report on a comprehensive proteomic analysis of EVs from different cell sources, including BM-MSC, found that the protein profiles of exosomes were more different from their cell of origin than from those of MVs. In addition, the exosome protein cargo was enriched in extracellular matrix and immune response proteins, whereas that of MVs was enriched in endoplasmic reticulum, proteasome and mitochondrial proteins. These investigators concluded that MVs and exosomes have different protein content despite the overlap in their size range [116]. To address the lack of markers for EV isolation and analysis, Kowal J. et al, conducted a quantitative proteomic analysis on four different fractions of EVs isolated from dendritic cells. Similarly, the findings by Haraszti et al, 2016, they concluded that mitochondria and proteasomes where mostly found in the 10,000 centrifugated pellet consistent with MVs, while extracellular matrix were specifically present in the 100,000 ultra-centrifugated pellet that was consistent with exosomes [117, 118]. These recent proteomic analysis reports highlight the fact that the protein content of both types of EVs (MVs and exosomes) may confer specific aspects of the ameliorating effects of hMSC EVs. We postulate that this is possibly through the paracrine effects of unique protein candidates acting in synergistically with other protein components through multiple pathways. One of the ways to test this hypothesis is through proteomic pathway analysis.

Pathway analysis following proteomic analysis are conducted to have a better understanding of the potential intracellular pathways associated with protein components of the

hMSC exosome proteome that may impart their beneficial effects. Many of these proteins, specifically enzymatic proteins that catalyze these biochemical reactions have been curated in pathway databases. One of the most widely used pathway databases is the Kyoto Encyclopedia of Genes and Genomes (KEGG). KEGG is a collection of knowledgebase databases that links large-scale molecular datasets, including proteomic analysis, to high-level cellular and biological systemic functions [119]. According to Kanehisa and colleagues, the KEGG PATHWAY database is key to the KEGG resource, containing annotated proteins classified with KEGG Annotation Analysis into sections, such as metabolism and cellular processes [120]. Therefore, this pathway database will be crucial in identifying key enzymatic proteins and their biochemical pathways following proteomic analysis of the hMSC exosome proteome.

Comprehensive (quantitative) proteomic analysis allows for absolute protein quantification that would be essential to compare the proteome of hMSC exosomes from different donors, however, previous knowledge on the protein composition (predefined peptides) is required for such an approach [121]. Moreover, there is limited data in the literature on the components of hMSC exosome proteome. Consequently, there is the need for of an initial descriptive proteomics, to identify key protein components that could be relevant in a future comprehensive comparative proteomic analysis. We therefore, sought to initially investigate the hMSC exosome proteome by qualitative proteomic analysis for potential protein components. We hypothesized that hMSC exosome proteome will contain protein components with proteolytic and antioxidative activities.

4.2 MATERIALS AND METHODS

4.2.1 Design

This was a descriptive proteomic analysis to identify and categorize the protein components of hMSC exosome proteome.

4.2.2 Source of human MSCs and exosome isolation

Well characterized BM-MSCs were obtained from the NHLBI-sponsored Production Assistance for Cellular Therapies (PACT) program based at the University of Minnesota, MN [91, 122]. Exosomes were isolated from these hMSCs as we and others have previously described [45, 92]. Briefly, hMSCs were cultured and expanded in DMEM media containing 15% FBS, 2% human serum and 2mM Glutamax in a T175 flask (ThermoFisher) to 80% confluency for the first and second passages. After the second passage, hMSCs were plated in multilayered tissue culture flasks (Millipore Sigma) in 400ml of maintenance media with exosome-depleted FBS (ThermoFisher) for exosome isolation. The 48 hours conditioned media from a total of 20 $X10^6$ hMSCs was collected and subjected to multiple differential ultracentrifugation steps as previously described [45, 93].

4.2.3 Pooling and purification of exosomes

The 8-10 isolates of crude exosomes from a single donor hMSCs, were pooled and purified over a 30% sucrose cushion in Tris/deuterium at 100,000g/ 2hrs as previously described by our group

and others [45, 93]. The pellets of the pooled samples were resuspended in 100ul of PBS and aliquots were taken for proteomic analysis, protein assay using a Micro BCA^{TM}Protein assay kit (ThermoFisher), and Nanosight Tracking Analysis (NTA) with a NanoSight LM10 for size distribution profile and concentrations (Malvern, Westborough, MA). The quality of the exosomes used for this proteomic analysis was determined to be good (427x 10^6 P/ug) based on the ratio of particle count (particles/ml by NTA) to protein concentration (ug/ml, micro BCR protein assay) of ≥300 x 10^6 P/ug according to Webber and Clayton [93](Figure 7).

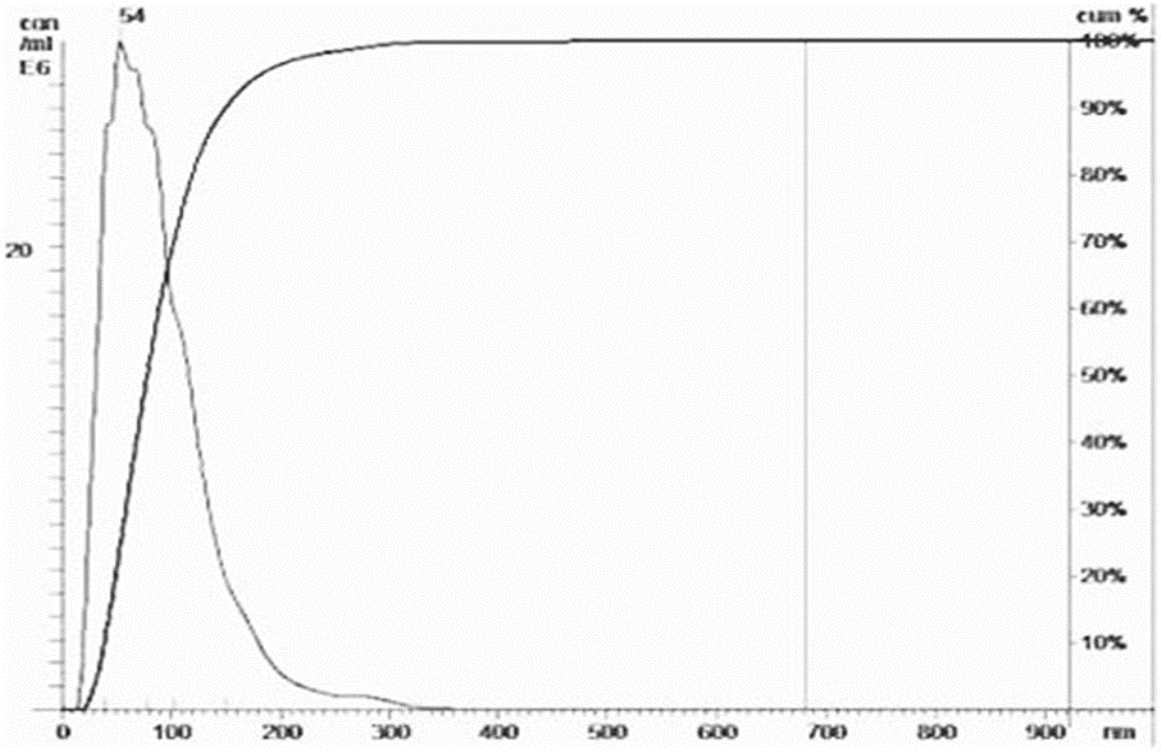

Figure 7 . hMSC exosome size distribution profile; mean size (90nm)

4.2.4 Sodium dodecyl sulfate–polyacrylamide gel electrophoresis and in-gel digestion

Protein extracts (100ug) from the pooled biological replicates of hMSCs exosomes were separated with a 1D sodium dodecyl sulfate–polyacrylamide gel electrophoresis **(**SDS-PAGE) on a 10% Bolt^{TM}-Tris Plus gel (ThermoFisher) under denaturing conditions in MOPS (3-N-Morpholinopropane Sulfonic acid) running buffer. Following staining in SimplyBlue^{TM} SafeStain (ThermoFisher), eight- 1mm cubic protein bands were cut per lane and placed in clean 1.5 ml Eppendorf tubes containing 100ul of double deionized H_20. The samples were then transmitted to the Biomedical Mass Spectrometry Center at the University of Pittsburgh for in-gel tryptic digestion followed by proteomic analysis.

4.2.5 Liquid chromatography tandem mass spectrometry

The in-gel tryptic digestion produced peptide mixtures that were analyzed by a reverse phase nano-HPLC coupled to an LTQ XL linear ion trap mass spectrometer (ThermoFisher) as described previously by the Yates group at the University of Pittsburgh Biomedical Mass Spectrometry Center [123] who performed the analysis. Briefly, full scan high resolution mass spectra were recorded at a rate of 1 spectrum/ sec. using a 300 Da to 2000 Da scan range. One microliter of digested sample was loaded with an autosampler onto a capillary sample trap column (100µm inner diameter (i.d) x 2.5cm) and desalted on line for 3 min at 3µL/min with solvent A [100% HPLC grade water, 0.1 Macetic acid]. After 4 minutes, the flow rate was reduced to 1 µl/min and peptides were eluted into an in-house packed spray tip column (100 µm i.d, 190µm outer diameter (o.d) × 8 cm). Thereafter, peptides were analyzed on an LTQ XL linear ion trap using a 75 min gradient run. The gradient was delivered by an Agilent 1100

capillary pump with four distinct sections; 90% Solvent B, followed by equilibration 100% A at 1μL/min from 60 to 75 min.

4.2.6 Identification of peptides and proteins

This was performed at the University of Pittsburgh Biomedical MS Center by very knowledgeable and skilled personnel in proteomic analysis as reported previously [123]. Briefly, the liquid chromatography tandem mass spectrometry (LC-MS/MS) spectra were acquired by data-dependent acquisition using 2 m/z isolation width. Each MS/MS product ion spectra were linked to a corresponding precursor ion feature, and DTA files were created for all precursor-linked MS/MS spectra from all raw data files. The DTA files were searched against Peptide Atlas database using the SEQUEST (Thermo Finnigan) search algorithms. Search parameters specified a tryptic enzyme cleavage at lysine or arginine, except when followed by a proline residue. A maximum of three missed cleavages were allowed within each peptide. Additional parameters included a precursor ion tolerance of ±80 parts per million (ppm), fragment ion tolerance of 0.5 Da, fixed alkylation of cysteine (+57.021 Da), variable oxidation of methionine (+15.9950 Da) and variable phosphorylation of serine, threonine, and tyrosine (+79.9660 Da). All other parameters were set to default SEQUEST values. Search result output files were submitted to a Prophets-based algorithm in Elucidator (Peptide Tellers) or Scaffold (Proteome Software) to create a statistical model for assigning cross-correlation values to peptide identifications. Filter settings were set to a predicted false discovery error rate of 0.005.

4.2.7 The Kyoto Encyclopedia of Genes and Genomes pathway analysis

The Kyoto Encyclopedia of Genes and Genomes **(**KEGG) enzyme database in the chemical information category was used to determine the protein enzyme composition of hMSCs and the chemical reactions they catalyze. KEEG is a collection of knowledgebase databases that link molecular datasets from high-throughput experiments, including proteomic analysis to high-level cellular and biological systemic functions [119]. According to these authors, the KEGG PATHWAY database is the core of the KEGG resource with annotated proteins classified into sections such as metabolism and cellular processes. The quality of databases is key to their utility as reference database. Since 2015, an addendum category was included in the KEEG database making it possible to collect protein sequence data from published literature as oppose to just relying on imported genome sequence from RefSeq. The information derived from chemical information category, facilitates the conversion of enzyme sets to a KEGG number set, enabling interpretation of high level biological processes.

4.2.8 Statistical analysis

Statistical analysis of large-scale proteomic data involves simultaneous, multiple hypotheses testing that is associated with an increased number of false positives. Multiple testing correction procedures are therefore required to address this issue. Estimating and controlling for the false discovery rate (FDR) was used as a multiple testing correction method [121].

The FDR method was first proposed by Benjamini and Hochberg [124] to correct for multiple testing errors. In this procedure, the individual uncorrected p-values were ranked from smallest to largest. The smallest or topmost p-value was ranked first, i=1, the next that follows is

second, i=2, etc. Afterwards, each individual p-value was compared to its calculated Benjamini-Hochberg (BH) critical value:(i/m) Q; where 'i' is the rank, 'm' is the total number of multiple tests, and Q is the chosen FDR, in this case 0.005. The first largest p-value on the list that was less than the BH critical value was considered significant and all other p-values smaller than the largest p-value were also reported as significant. In proteomic analysis, the FDR is controlled for during the peptide identification and protein assembly phases.

At the peptide identification phase, the SEQUEST search algorithm identifies each tandem mass spectrum that represents an individual peptide. The SEQUEST program then uses this information to search against a knowledgebase protein database for candidate peptide sequences that match the observed spectrum. These theoretical spectra, from the database, were matched to the observed mass spectrum by cross-correlation assessments, which is a measure of the similarity between two spectra. This process involved multiple hypotheses testing to generate a ranked list of peptide-spectra matches (PSMs) based on the cross-correlation scores with their corresponding uncorrected p-values. The p-value for a given target PSM cross-correlation score (s), was determined by calculating the percentage of decoy (from the decoy database) PSMs that received the same score or higher (≥s). The null model here is the lack of a match between target PSM and decoy PSM scores [125].

At the protein assembly phase of the proteomic analysis, the tandem MS spectra are matched to the amino acid sequence of specific peptides whose patterns are used to determine their parent proteins. Annotated knowledgebase programs such as the KEGG database are then used to elicit their role in biological processes. The KEEGG pathway enrichment analysis identifies proteins from the input raw data lists that are enriched in a pathway associated with a phenotype. We tested the sample-level [126] null hypothesis that gene products (proteins) of a

pathway (first dataset) are no more associated to a phenotype than non-pathway (second dataset) proteins. A hypergeometric test was used to test this hypothesis with their corresponding uncorrected p-values [127]. The Benjamini-Hochberg procedure was then applied to adjusts these uncorrected p-values to control for FDRs as described above.

4.3 RESULTS

We identified a total of 845 proteins in our hMSC exosome sample. Using the KEGG pathway program, the identified proteins were mapped to specific biological pathways (Table 5). Proteins associated with arrhythmogenic RV cardiomyocytes, ECM receptor interactions and proteasomes made up the 5-topmost all protein groups. Out of these, 166 were enzymatic proteins of which proteasomes, glycolysis/gluconeogenesis, and pentose phosphate pathway proteins were among the 4-topmost biological processes.

Table 5 A. All 845 identified proteins; B. Main biological processes of the 166 identified enzymes

A.

Term	#	%	P-Value	Benjamani
Complement and coagulation cascades	**37**	**4.4**	**7.50E-22**	**1.10E-19**
Regulation of actin cytoskeleton	47	5.6	5.50E-10	4.10E-08
Arrhythmogenic right ventricular cardiomyopathy (ARVC)	25	3	3.10E-09	1.50E-07
ECM-receptor interaction	26	3.1	5.70E-09	2.10E-07
Proteasome	**18**	**2.2**	**6.80E-08**	**2.00E-06**
Hypertrophic cardiomyopathy (HCM)	24	2.9	1.70E-07	4.20E-06
Dilated cardiomyopathy	25	3	1.90E-07	4.10E-06
Focal adhesion	40	4.8	2.10E-07	3.90E-06
Pathogenic Escherichia coli infection	19	2.3	3.00E-07	5.00E-06
Leukocyte transendothelial migration	28	3.3	5.90E-07	8.80E-06
Endocytosis	35	4.2	4.10E-06	5.60E-05
Ribosome	22	2.6	4.40E-06	5.50E-05
Systemic lupus erythematosus	23	2.8	1.10E-05	1.30E-04
Prion diseases	13	1.6	1.20E-05	1.20E-04
SNARE interactions in vesicular transport	13	1.6	3.00E-05	3.00E-04
Vibrio cholerae infection	**15**	**1.8**	**1.20E-04**	**1.10E-03**
Glycolysis / Gluconeogenesis	**14**	**1.7**	**9.10E-04**	**8.00E-03**
Cell adhesion molecules (CAMs)	22	2.6	2.20E-03	1.80E-02
Adherens junction	15	1.8	3.50E-03	2.70E-02
Neurotrophin signaling pathway	20	2.4	5.40E-03	4.00E-02
Epithelial cell signaling in Helicobacter pylori infection	**13**	**1.6**	**8.40E-03**	**5.80E-02**
Hematopoietic cell lineage	15	1.8	9.50E-03	6.30E-02
Gap junction	15	1.8	1.30E-02	8.00E-02
Pentose phosphate pathway	**7**	**0.8**	**1.40E-02**	**8.20E-02**
Axon guidance	19	2.3	1.70E-02	9.90E-02

B.

Term	#	%	P-Value	Benjamani
Proteasome	**13**	**7.8**	**3.30E-10**	**2.80E-08**
Glycolysis / Gluconeogenesis	**13**	**7.8**	**6.90E-09**	**2.90E-07**
Complement and coagulation cascades	11	6.6	3.10E-06	8.60E-05
Pentose phosphate pathway	**7**	**4.2**	**1.60E-05**	**3.40E-04**
Epithelial cell signaling in Helicobacter pylori infection	9	5.4	1.40E-04	2.40E-03
Vibrio cholerae infection	**8**	**4.8**	**2.60E-04**	**3.60E-03**
Starch and sucrose metabolism	7	4.2	3.50E-04	4.20E-03
Nicotinate and nicotinamide metabolism	5	3	2.00E-03	2.10E-02
Glutathione metabolism	6	3.6	5.50E-03	5.00E-02
Amino sugar and nucleotide sugar metabolism	5	3	1.80E-02	1.40E-01
Folate biosynthesis	3	1.8	2.50E-02	1.80E-01
Citrate cycle (TCA cycle)	**4**	**2.4**	**3.30E-02**	**2.10E-01**
Porphyrin and chlorophyll metabolism	4	2.4	3.90E-02	2.30E-01
Cysteine and methionine metabolism	4	2.4	4.20E-02	2.30E-01
Renin-angiotensin system	3	1.8	5.70E-02	2.80E-01
Purine metabolism	8	4.8	6.20E-02	2.80E-01
Pyruvate metabolism	4	2.4	6.30E-02	2.80E-01
Oxidative phosphorylation	7	4.2	7.80E-02	3.20E-01
Phenylalanine metabolism	3	1.8	9.00E-02	3.40E-01

The major enzyme groups were hydrolases (48.2%) followed by transferases (21.1%) and oxidoreductases (16.3%) (Table 6).

Table 6 Distribution of enzymes by class in hMSC exosome proteome

Classes of enzymes	%	Number of proteins
Hydrolase	48.2	81
Transferase	21.1	34
Oxidoreductase	16.3	27
Isomerase	6.6	11
Lyase	5.4	9
Ligase	2.4	4
Total	100	**166**

Enzymes are known to regulate many biological processes such as cellular bioenergetics and extracellular matrix turnover. In assessing the enzymatic activities (Figure 8), 57% of the hydrolases acted on peptide bonds (proteinases) and 15% on acid anhydride bonds (ATPases). Most of the hydrolases comprised proteasomes (PSMA, PSMB), extracellular matrix metalloproteinases (MMP2, MMP14) and ATPase (ATP2B4) that have been reported to be associated with ECM turnover and cardiac remodeling [67]. This suggest that hMSC exosome carry enzymatic proteins that could be transferred to target cells, including cardiopulmonary cells to change their phenotype for tissue repair.

Of the transferases, 29% were phosphotransferases, 26% glycosyltransferases, and 18% acyltransferases. Moreover, key enzymes of the glycolytic pathway such as pyruvate kinase (PKM1) and phosphoglycerate kinase (PGK1) were also identified. This indicates that hMSC exosomes are vectors of enzymes that could be internalized by target cells to modulate their bioenergetics.

With regards to the oxidoreductases, 26% were CH-OH donors such as malate dehydrogenase (MDH1), an important NADP generator, 19% peroxide acceptors, and almost half (40%) were

grouped as miscellaneous, which included lysyl oxidase (LOX) a crucial enzyme involved in cross-liking collagen fibrils to stabilize the ECM. Importantly, a peroxide acceptor, glutathione peroxidase 3 (GPX3) was identified in our hMSC exosome sample. Glutathione peroxidase 3 is important in protecting cells against oxidative stress damage.

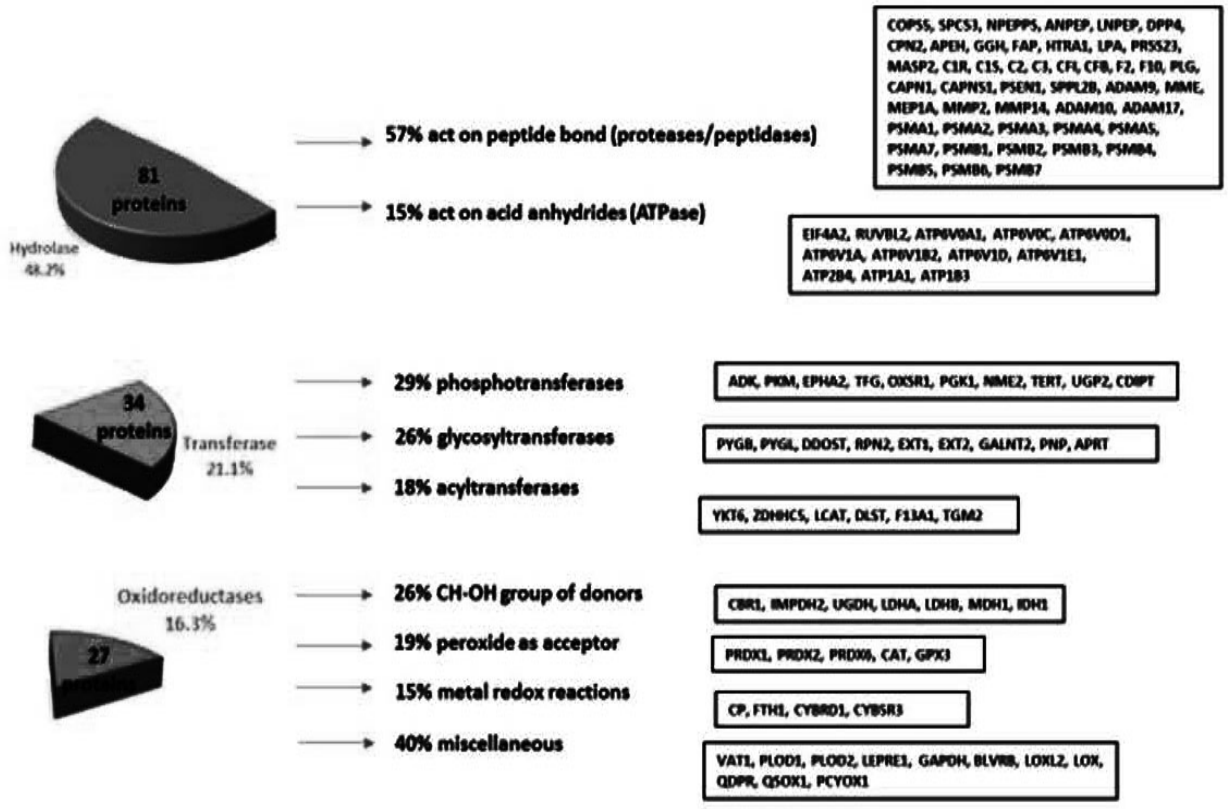

Figure 8 Distribution of enzymes by class in hMSC exosome proteome with their protein symbols

Collectively, these enzymatic proteins have the potential to inhibit and scavenge excessive ROS generation (glutathione peroxidase and pentose phosphate pathway), regulate ECM turnover (proteasomes, matrix metalloproteinases, and lysyl oxidase), and modulate the bioenergetic phenotype of target cells through glycolysis (pyruvate kinase).

4.4 DISCUSSIONS

In our descriptive proteomic analysis, we identified 845 distinct proteins and of these, 166 (19.6%) were categorized as enzymes. Enzymes are proteins that are well known to catalyze biochemical reactions and have the potential to alter biological processes in cells. There is increasing evidence that a reasonable number of proteins in exosomes have enzymatic functions [66].

Our proteomic pathway analysis identified proteins that were associated with the 5-topmost biological processes, which included arrhythmogenic RV cardiomyocytes, ECM receptor interactions and proteolytic proteasomes. Of the enzymatic groups identified, the hydrolases comprised proteasomes, extracellular matrix metalloproteinases, and ATPase that have implications in ECM turnover and cardiac remodeling [67]. This data is consistent with reports by Lai R. et al, who found 857 proteins in the proteomic analysis of the hMSC exosome proteome and demonstrated that 20S proteasome was the 8th predominant protein component. Just as Lai R. et al, we found all seven alpha and beta subunits of the 20S proteasome in our proteomic data (Figure 3). The authors also detected an overrepresentation of all seven alpha (PSMA) and beta (PSMB) subunits of the 20S proteasome that confers the catalytic properties of the parent 26S proteasome in their proteome [66]. Furthermore, they showed that the 20S proteasome subunit was responsible for the degradation of 90% of all intracellular oxidatively damaged proteins [66]. The publication by Lai R. et al was specifically focused on the proteolytic potential of hMSC exosomes proteasomes, in the backdrop of a report that some alpha/beta hydrolase fold superfamily members lack enzymatic activities [128]. Interestingly, proteasomes have been demonstrated to have extracellular proteolytic activities in an ATP/ ubiquitin-independent manner in alveolar fluid of patients with inflammatory lung diseases [65]. Proteasomes

may, therefore, play a pivotal role in clearing both intracellular and extracellular misfolded proteins [63, 65], which have widely been proven to mediate cell death and tissue dysfunction. Put together, hMSC exosomes carry protein mediators with proteolytic potential that could clear misfolded intracellular proteins and proteinaceous extracellular debris to mitigate cell death and inflammation. These extracellular proteolytic activities of proteasomes may be enhanced by traditional extracellular matrix (ECM) enzymes such as matrix metalloproteinases (MMPs).

A major group of MMPs known to play a crucial role in ECM clearance are the gelatinases, MMP2 and MMP9 [115, 129]. In our hMSC exosome sample, we found MMP2 and its activator, membrane type-1 MMP (MMP14). In 2012, Kim Han-Soo and collaborators, showed that proteolysis was the fourth topmost biological process in the proteome of hMSC microvesicles [114]. Other investigators working on the proteomic analysis of hMSC extracellular vesicles have demonstrated the enrichment of ECM pathway proteins in hMSC exosomes [116, 117].Most recently, Anderson J. et al, conducted a quantitative proteomic analysis of human BM-MSC exosomes and revealed their modulatory properties in angiogenesis. They further demonstrated that the proteome of hMSC exosomes contained an enriched profile of angiogenic signaling proteins that were capable of inducing angiogenesis [115]. Taken together, hMSC exosomes contain proteasomes and angiogenic signaling molecules that are capable of mediating angiogenesis. These are key elements for any therapeutic agent that might be useful in mitigating RV and pulmonary remodeling.

Similarly, in their report on a comprehensive proteomic analysis of EVs from different cell sources, including BM-MSC, Haraszti RA and colleagues found that the protein profiles of exosomes were more different from their parent cell than those of MVs. According to these investigators, the exosome protein cargo was enriched in extracellular matrix and immune

response proteins whereas, that of MVs were enriched in endoplasmic reticulum, mitochondrial proteins and proteasomes [116]. Therefore, both types of EVs (MVs and exosomes) carry subcellular components with unique therapeutic potentials. Interestingly, Kowal J. et al, conducted a comparative quantitative proteomic analysis on four different fractions of EVs obtained from dendritic cells to evaluate potential markers for EV isolation and analysis [117]. Surprisingly, they confirmed the findings by Haraszti et al, 2016, by demonstrating that mitochondria and proteasomes where mostly found in MVs, while extracellular matrix was specifically present in exosomes [117, 118]. Collectively, these recent proteomic analyses demonstrate that both types of EVs carry protein components or subcellular organelles that can act synergistically to confer the most optimal therapeutic effects to repair damaged tissue. Potency in their therapeutic effects may also be augmented by acting in concert with other classes of enzymes such as oxidoreductases.

The oxidoreductases malate dehydrogenase (MDH1) and glutathione peroxidase 3 (GPX3), nicotinamide adenine dinucleotide phosphate ($NADP^+$) and peroxide acceptors, were identified in our proteomic analysis. Importantly, the pentose phosphate pathway (PPP) was identified as one of the top four catalyzed biological processes. This indicates hMSC exosomes carry enzyme proteins that could modulate cellular oxidative stress. The PPP continuously generates reduced $NADP^+$ (NADPH), which is an essential cofactor in antioxidant pathways [62]. NADPH act as an electron donor to glutathione reductase in its catalytic reduction of glutathione (GSSG) to reduced glutathione (GSH), a crucial reaction in modulating oxidative stress. When more free radicals are generated than can be quenched, there is an ensuing oxidative stress that is deleterious to the mitochondria and the entire cell [130]. Moreover, in a recent report from our group, we showed that hMSCs extracellular vesicles mediate the restoration of mitochondrial

function, a key source of cellular ROS, in targeted cells [45]. This report was consistent with our previous publication that showed that TNF induced an increase in both phagocytic (NADPH oxidase-NOX) and mitochondrial ROS generation [131]. Despite the dearth of data on hMSC exome proteome and their antioxidant potential, a recent article showed that the pentose phosphate pathway (PPP) was enriched in exosome isolated from ovarian cancer cell lines [132]. These investigators asserted that PPP created a metabolic shift to glycolysis that may promote tumor metastasis but based on the several reported beneficial effects of hMSC exosomes in a wide range of diseases, we postulated that hMSC exosomes are most likely to modulate the antioxidant pathway through an increased generation of NADPH from the PPP. Collectively, these data highlight the potential role of hMSC exosomes as conveyors of antioxidant effectors. The reparative antioxidant potential of hMSC exosome can be enhanced synergistically by the presence in hMSC exosomes of proteolytic factors. Together, these data suggest that hMSC exosome have the potential to exert optimal pleiotropic therapeutic effects through the synergistic actions of various components of the hMSC exosome proteome, including modulating ECM turnover and oxidative stress as well as the proteolytic activities of proteasomes and MMPs to facilitate tissue repair and regeneration.

Limitations. The current isolation and purification techniques are still insufficient to clearly distinguish between exosomes and MVs based on their physical and biochemical properties. Therefore, it is very likely that our hMSC exosome samples may contain some MVs. Despite this limitation, there is a growing number of investigators including our group, who postulate a complementary beneficial effect in the combined administration of exosomes and MVs for tissue repair.

We performed a descriptive, qualitative proteomic analysis that inherently, lacks the ability to provide relative or absolute quantification of the identified proteins. Nonetheless, descriptive proteomic analysis is critical to identifying key protein candidates that could be further analyzed by a comprehensive comparative proteomic analysis.

5.0 CONCLUSIONS

The analysis of the data from our first project on the IPF registry, showed that pulmonary hypertension (PH) and right ventricular systolic dysfunction (RVSD) are prevalent and strongly associated with survival in IPF.RHC assessments of the RV function in IPF is an important modality i to identify patients that are at risk of worse outcomes who may be considered for to benefit from novel treatment options in clinical trials.

Based on the results from our second project, we concluded that hMSCs and their derived exosomes have the therapeutic potential to improve RV adaptive contractility. Their modulatory effects on the RV function within the context of fibrotic lung disease may improve outcomes, judging from the demonstrated strong association between RV function and survival.

Lastly in our third project, we concluded that the proteome of hMSC exosome carry enzymatic proteins that can mediate the therapeutic effects of stem cell-based therapies. Importantly, that the synergistic actions of their antioxidative, ECM turnover and proteolytic properties is a potential mechanism employed to enhance their therapeutic effects in a wide range of diseases, including fibrotic lung diseases.

6.0 FUTURE DIRECTIONS

A large Pennsylvania-statewide IPF registry study will be required to validate our cutoff value for RVD, which should be evaluated as an important factor in the development of a composite score for predicting outcomes in IPF.

In our second aim, a dose-escalation in vivo experimental design, over a longer exposure period will be necessary to investigate the dose-dependent effect of the efficacy of hMSCs and their derived exosomes. This will allow for the assessment of the transition from adaptive, compensated RV dysfunction to overt, maladaptive, decompensated RV failure.

Our descriptive proteomic analysis findings have laid the foundation for a future comprehensive proteomic analysis study that will focus on the key catalytic proteins that were identified. Furthermore, it will be important to investigate the hMSC exosome proteome from multiple human donors to compared differentially expressed proteins. This has the potential to guide the bioengineering of enriched exosomes that could convey key protein components for targeted tissue repair, screening for biomarkers of hMSC exosome potency, and for advancing the understanding hMSC exosome pathobiology.

Appendix A

Table 7 Meaning of acronyms and abbreviations

Aconyms and abbreviations	Full meaning
BFLI	Bleomycin-induced fibrotic lung injury
FLI	Fibrotic lung injury
CO	Cardiac output
dP/dt_{mx}-EDV	Maximum systolic pressure derivative
dP/dt_{mx}-EDV	Maximum systolic pressure derivative to end-diastolic volume
E_a	Pulmonary effective elastance
E_{es}	End-systolic ventricular elastance
EDV	End-diastolic volume
EF	Ejection fraction
ESPVR	End-systolic pressure volume relationship
hMSCs	Human mesenchymal stem cells
MSCs	Mesenchymal stem cells
mPAP	Mean pulmonary arterial pressure
PV loop	Pressure-Volume loop
PRSW	stroke work
PVR	Pulmonary vascular resistance
RVSP	Right ventricular systolic pressure
RVD	Right ventricular dysfunction
RVSD	Right ventricular systolic dysfunction
SV	Stroke volume
SVI	Stroke volume index

BIBLIOGRAPHY

1. Raghu, G. *et al.* An official ATS/ERS/JRS/ALAT statement: idiopathic pulmonary fibrosis: evidence-based guidelines for diagnosis and management. *American journal of respiratory and critical care medicine* **183**, 788-824 (2011).

2. Fernandez Perez, E.R. *et al.* Incidence, prevalence, and clinical course of idiopathic pulmonary fibrosis: a population-based study. *Chest* **137**, 129-137 (2010).

3. Raghu, G., Weycker, D., Edelsberg, J., Bradford, W.Z. & Oster, G. Incidence and prevalence of idiopathic pulmonary fibrosis. *American journal of respiratory and critical care medicine* **174**, 810-816 (2006).

4. Vonk-Noordegraaf, A. *et al.* Right heart adaptation to pulmonary arterial hypertension: physiology and pathobiology. *Journal of the American College of Cardiology* **62**, D22-33 (2013).

5. D'Andrea, A. *et al.* Right ventricular strain: An independent predictor of survival in idiopathic pulmonary fibrosis. *International journal of cardiology* **222**, 908-910 (2016).

6. Monsel, A., Zhu, Y.G., Gudapati, V., Lim, H. & Lee, J.W. Mesenchymal stem cell derived secretome and extracellular vesicles for acute lung injury and other inflammatory lung diseases. *Expert opinion on biological therapy* **16**, 859-871 (2016).

7. Glassberg, M.K. *et al.* Allogeneic human mesenchymal stem cells in patients with idiopathic pulmonary fibrosis via intravenous delivery (AETHER): a phase I, safety, clinical trial. *Chest* (2016).

8. Tsao, C.R., Liao, M.F., Wang, M.H., Cheng, C.M. & Chen, C.H. Mesenchymal Stem Cell Derived Exosomes: A New Hope for the Treatment of Cardiovascular Disease? *Acta Cardiologica Sinica* **30**, 395-400 (2014).

9. van Wolferen, S.A. *et al.* Prognostic value of right ventricular mass, volume, and function in idiopathic pulmonary arterial hypertension. *European Heart Journal* **28**, 1250-1257 (2007).

10. Vonk Noordegraaf, A., Westerhof, B.E. & Westerhof, N. The Relationship Between the Right Ventricle and its Load in Pulmonary Hypertension. *Journal of the American College of Cardiology* **69**, 236-243 (2017).

11. Galiè, N. & Simonneau, G. The Fifth World Symposium on Pulmonary Hypertension. *Journal of the American College of Cardiology* **62**, D1 (2013).

12. Galie, N. *et al.* Guidelines for the diagnosis and treatment of pulmonary hypertension: The Task Force for the Diagnosis and Treatment of Pulmonary Hypertension of the European Society of Cardiology (ESC) and the European Respiratory Society (ERS), endorsed by the International Society of Heart and Lung Transplantation (ISHLT). *Eur Heart J* **30**, 2493-2537 (2009).

13. Nathan, S.D., Noble, P.W. & Tuder, R.M. Idiopathic pulmonary fibrosis and pulmonary hypertension: connecting the dots. *American journal of respiratory and critical care medicine* **175**, 875-880 (2007).

14. Kawut, S.M. *et al.* Exercise testing determines survival in patients with diffuse parenchymal lung disease evaluated for lung transplantation. *Respiratory medicine* **99**, 1431-1439 (2005).

15. Rivera-Lebron, B.N. *et al.* Echocardiographic and hemodynamic predictors of mortality in idiopathic pulmonary fibrosis. *Chest* **144**, 564-570 (2013).

16. Raghu, G. *et al.* An Official ATS/ERS/JRS/ALAT Clinical Practice Guideline: Treatment of Idiopathic Pulmonary Fibrosis. An Update of the 2011 Clinical Practice Guideline. *American journal of respiratory and critical care medicine* **192**, e3-19 (2015).

17. du Bois, R.M. *et al.* Forced vital capacity in patients with idiopathic pulmonary fibrosis: test properties and minimal clinically important difference. *American journal of respiratory and critical care medicine* **184**, 1382-1389 (2011).

18. Ley, B., Collard, H.R. & King, T.E., Jr. Clinical course and prediction of survival in idiopathic pulmonary fibrosis. *American journal of respiratory and critical care medicine* **183**, 431-440 (2011).

19. Paterniti, M.O. *et al.* Acute Exacerbation and Decline in Forced Vital Capacity Are Associated with Increased Mortality in Idiopathic Pulmonary Fibrosis. *Annals of the American Thoracic Society* (2017).

20. Voelkel, N.F. *et al.* Right ventricular function and failure: report of a National Heart, Lung, and Blood Institute working group on cellular and molecular mechanisms of right heart failure. *Circulation* **114**, 1883-1891 (2006).

21. Simon, M.A. & Pinsky, M.R. Right ventricular dysfunction and failure in chronic pressure overload. *Cardiology research and practice* **2011**, 568095 (2011).

22. Vanderpool, R.R. *et al.* RV-pulmonary arterial coupling predicts outcome in patients referred for pulmonary hypertension. *Heart (British Cardiac Society)* **101**, 37-43 (2015).

23. Overbeek, M.J. *et al.* Right ventricular contractility in systemic sclerosis-associated and idiopathic pulmonary arterial hypertension. *The European respiratory journal* **31**, 1160-1166 (2008).

24. Naeije, R. & Manes, A. The right ventricle in pulmonary arterial hypertension. *European respiratory review : an official journal of the European Respiratory Society* **23**, 476-487 (2014).

25. Kubba, S., Davila, C.D. & Forfia, P.R. Methods for Evaluating Right Ventricular Function and Ventricular-Arterial Coupling. *Progress in cardiovascular diseases* **59**, 42-51 (2016).

26. Spruijt, O.A. *et al.* The effects of exercise on right ventricular contractility and right ventricular-arterial coupling in pulmonary hypertension. *American journal of respiratory and critical care medicine* **191**, 1050-1057 (2015).

27. Wauthy, P., Pagnamenta, A., Vassalli, F., Naeije, R. & Brimioulle, S. Right ventricular adaptation to pulmonary hypertension: an interspecies comparison. *American journal of physiology. Heart and circulatory physiology* **286**, H1441-1447 (2004).

28. Lazo, J.S., Hoyt, D.G., Sebti, S.M. & Pitt, B.R. Bleomycin: a pharmacologic tool in the study of the pathogenesis of interstitial pulmonary fibrosis. *Pharmacology & therapeutics* **47**, 347-358 (1990).

29. Braun, R.K. *et al.* Comparison of two models of bleomycin-induced lung fibrosis in mouse on the level of leucocytes and T cell subpopulations in bronchoalveolar lavage. *Comparative Haematology International* **6**, 141-148 (1996).

30. Hemnes, A.R., Zaiman, A. & Champion, H.C. PDE5A inhibition attenuates bleomycin-induced pulmonary fibrosis and pulmonary hypertension through inhibition of ROS generation and RhoA/Rho kinase activation. *American journal of physiology. Lung cellular and molecular physiology* **294**, L24-33 (2008).

31. Srour, N. & Thebaud, B. Mesenchymal Stromal Cells in Animal Bleomycin Pulmonary Fibrosis Models: A Systematic Review. *Stem cells translational medicine* **4**, 1500-1510 (2015).

32. Dominici, M. *et al.* Minimal criteria for defining multipotent mesenchymal stromal cells. The International Society for Cellular Therapy position statement. *Cytotherapy* **8**, 315-317 (2006).

33. Prockop, D.J. Inflammation, fibrosis, and modulation of the process by mesenchymal stem/stromal cells. *Matrix biology: journal of the International Society for Matrix Biology* **51**, 7-13 (2016).

34. Friedenstein, A.J., Chailakhjan, R.K. & Lalykina, K.S. The development of fibroblast colonies in monolayer cultures of guinea-pig bone marrow and spleen cells. *Cell and tissue kinetics* **3**, 393-403 (1970).

35. Toonkel, R.L., Hare, J.M., Matthay, M.A. & Glassberg, M.K. Mesenchymal stem cells and idiopathic pulmonary fibrosis. Potential for clinical testing. *American journal of respiratory and critical care medicine* **188**, 133-140 (2013).

36. Weiss, D.J. & Ortiz, L.A. Cell therapy trials for lung diseases: progress and cautions. *American journal of respiratory and critical care medicine* **188**, 123-125 (2013).

37. Matthay, M.A. *et al.* Cell therapy for lung diseases. Report from an NIH-NHLBI workshop, November 13-14, 2012. *American journal of respiratory and critical care medicine* **188**, 370-375 (2013).

38. Chambers, D.C. *et al.* A phase 1b study of placenta-derived mesenchymal stromal cells in patients with idiopathic pulmonary fibrosis. *Respirology (Carlton, Vic.)* **19**, 1013-1018 (2014).

39. Squillaro, T., Peluso, G. & Galderisi, U. Clinical Trials with Mesenchymal Stem Cells: An Update. *Cell transplantation* **25**, 829-848 (2016).

40. Lee, R.H. *et al.* TSG-6 as a biomarker to predict efficacy of human mesenchymal stem/progenitor cells (hMSCs) in modulating sterile inflammation in vivo. *Proceedings of the National Academy of Sciences of the United States of America* **111**, 16766-16771 (2014).

41. Russell, K.C. *et al.* Clonal analysis of the proliferation potential of human bone marrow mesenchymal stem cells as a function of potency. *Biotechnology and bioengineering* **108**, 2716-2726 (2011).

42. Lee, R.H. *et al.* Intravenous hMSCs improve myocardial infarction in mice because cells embolized in lung are activated to secrete the anti-inflammatory protein TSG-6. *Cell stem cell* **5**, 54-63 (2009).

43. Stabler, C.T., Lecht, S., Lazarovici, P. & Lelkes, P.I. Mesenchymal stem cells for therapeutic applications in pulmonary medicine. *British medical bulletin* **115**, 45-56 (2015).

44. Akram, K.M., Patel, N., Spiteri, M.A. & Forsyth, N.R. Lung Regeneration: Endogenous and Exogenous Stem Cell Mediated Therapeutic Approaches. *International journal of molecular sciences* **17** (2016).

45. Phinney, D.G. *et al.* Mesenchymal stem cells use extracellular vesicles to outsource mitophagy and shuttle microRNAs. *Nature communications* **6**, 8472 (2015).

46. Quesenberry, P.J., Aliotta, J., Deregibus, M.C. & Camussi, G. Role of extracellular RNA-carrying vesicles in cell differentiation and reprogramming. *Stem cell research & therapy* **6**, 153 (2015).

47. van Doormaal, F.F., Kleinjan, A., Di Nisio, M., Buller, H.R. & Nieuwland, R. Cell-derived microvesicles and cancer. *The Netherlands journal of medicine* **67**, 266-273 (2009).

48. Raposo, G. & Stoorvogel, W. Extracellular vesicles: Exosomes, microvesicles, and friends. *The Journal of cell biology* **200**, 373-383 (2013).

49. Collino, F. *et al.* Microvesicles derived from adult human bone marrow and tissue specific mesenchymal stem cells shuttle selected pattern of miRNAs. *PloS one* **5**, e11803 (2010).

50. Crescitelli, R. *et al.* Distinct RNA profiles in subpopulations of extracellular vesicles: apoptotic bodies, microvesicles and exosomes. *J Extracell Vesicles* **2** (2013).

51. Champion, H.C., Michelakis, E.D. & Hassoun, P.M. Comprehensive Invasive and Noninvasive Approach to the Right Ventricle–Pulmonary Circulation Unit. *Circulation* **120**, 992 (2009).

52. Dimmeler, S., Ding, S., Rando, T.A. & Trounson, A. Translational strategies and challenges in regenerative medicine. *Nature medicine* **20**, 814-821 (2014).

53. Basu, J. & Ludlow, J.W. Exosomes for repair, regeneration and rejuvenation. *Expert opinion on biological therapy* **16**, 489-506 (2016).

54. Arslan, F. *et al.* Mesenchymal stem cell-derived exosomes increase ATP levels, decrease oxidative stress and activate PI3K/Akt pathway to enhance myocardial viability and prevent adverse remodeling after myocardial ischemia/reperfusion injury. *Stem Cell Res* **10**, 301-312 (2013).

55. Aliotta, J.M. *et al.* Exosomes induce and reverse monocrotaline-induced pulmonary hypertension in mice. *Cardiovascular research* **110**, 319-330 (2016).

56. Lee, C. *et al.* Exosomes mediate the cytoprotective action of mesenchymal stromal cells on hypoxia-induced pulmonary hypertension. *Circulation* **126**, 2601-2611 (2012).

57. Gonzalez-Gonzalez, F.J., Chandel, N.S., Jain, M. & Budinger, G.R.S. Reactive oxygen species as signaling molecules in the development of lung fibrosis. *Translational research : the journal of laboratory and clinical medicine* **190**, 61-68 (2017).

58. Sutendra, G. *et al.* A metabolic remodeling in right ventricular hypertrophy is associated with decreased angiogenesis and a transition from a compensated to a decompensated state in pulmonary hypertension. *Journal of molecular medicine (Berlin, Germany)* **91**, 1315-1327 (2013).

59. Rawat, D.K. *et al.* Increased Reactive Oxygen Species, Metabolic Maladaptation, and Autophagy Contribute to Pulmonary Arterial Hypertension–Induced Ventricular Hypertrophy and Diastolic Heart Failure. *Hypertension* **64**, 1266 (2014).

60. Redout, E.M. *et al.* Right-ventricular failure is associated with increased mitochondrial complex II activity and production of reactive oxygen species. *Cardiovascular research* **75**, 770-781 (2007).

61. Bocchino, M. *et al.* Reactive oxygen species are required for maintenance and differentiation of primary lung fibroblasts in idiopathic pulmonary fibrosis. *PloS one* **5**, e14003 (2010).

62. Mercer, J.R. Mitochondrial bioenergetics and therapeutic intervention in cardiovascular disease. *Pharmacology & therapeutics* **141**, 13-20 (2014).

63. Grimm, S., Hohn, A. & Grune, T. Oxidative protein damage and the proteasome. *Amino acids* **42**, 23-38 (2012).

64. Wang, X. *et al.* Mass spectrometric characterization of the affinity-purified human 26S proteasome complex. *Biochemistry* **46**, 3553-3565 (2007).

65. Sixt, S.U. & Peters, J. Extracellular alveolar proteasome: possible role in lung injury and repair. *Proceedings of the American Thoracic Society* **7**, 91-96 (2010).

66. Lai, R.C. *et al.* Proteolytic Potential of the MSC Exosome Proteome: Implications for an Exosome-Mediated Delivery of Therapeutic Proteasome. *International Journal of Proteomics* **2012**, 14 (2012).

67. Prathipati, P., Nandi, S.S. & Mishra, P.K. Stem Cell-Derived Exosomes, Autophagy, Extracellular Matrix Turnover, and miRNAs in Cardiac Regeneration during Stem Cell Therapy. *Stem cell reviews* **13**, 79-91 (2017).

68. Nathan, S.D. *et al.* Right ventricular systolic pressure by echocardiography as a predictor of pulmonary hypertension in idiopathic pulmonary fibrosis. *Respiratory medicine* **102**, 1305-1310 (2008).

69. Vonk-Noordegraaf, A. & Westerhof, N. Describing right ventricular function. *The European respiratory journal* **41**, 1419-1423 (2013).

70. Sagawa, K. The end-systolic pressure-volume relation of the ventricle: definition, modifications and clinical use. *Circulation* **63**, 1223-1227 (1981).

71. Brimioulle, S. *et al.* Single-beat estimation of right ventricular end-systolic pressure-volume relationship. *American journal of physiology. Heart and circulatory physiology* **284**, H1625-1630 (2003).

72. Kalogeropoulos, A.P., Vega, J.D., Smith, A.L. & Georgiopoulou, V.V. Pulmonary hypertension and right ventricular function in advanced heart failure. *Congestive heart failure (Greenwich, Conn.)* **17**, 189-198 (2011).

73. O'Brien, E.C. *et al.* Rationale for and design of the Idiopathic Pulmonary Fibrosis-PRospective Outcomes (IPF-PRO) registry. *BMJ open respiratory research* **3**, e000108 (2016).

74. Jo, H.E. *et al.* Baseline characteristics of idiopathic pulmonary fibrosis: analysis from the Australian Idiopathic Pulmonary Fibrosis Registry. *The European respiratory journal* **49** (2017).

75. Behr, J. *et al.* Management of patients with idiopathic pulmonary fibrosis in clinical practice: the INSIGHTS-IPF registry. *The European respiratory journal* **46**, 186-196 (2015).

76. Ferrara, G. *et al.* Idiopathic pulmonary fibrosis in Sweden: report from the first year of activity of the Swedish IPF-Registry. *European clinical respiratory journal* **3**, 31090 (2016).

77. ATS/ERS American Thoracic Society/European Respiratory Society International Multidisciplinary Consensus Classification of the Idiopathic Interstitial Pneumonias. This joint statement of the American Thoracic Society (ATS), and the European Respiratory Society (ERS) was adopted by the ATS board of directors, June 2001 and by the ERS Executive Committee, June 2001. *American journal of respiratory and critical care medicine* **165**, 277-304 (2002).

78. Lakatos, E. & Lan, K.K. A comparison of sample size methods for the logrank statistic. *Statistics in medicine* **11**, 179-191 (1992).

79. Lettieri, C.J., Nathan, S.D., Barnett, S.D., Ahmad, S. & Shorr, A.F. Prevalence and outcomes of pulmonary arterial hypertension in advanced idiopathic pulmonary fibrosis. *Chest* **129**, 746-752 (2006).

80. Nathan, S.D. *et al.* Serial development of pulmonary hypertension in patients with idiopathic pulmonary fibrosis. *Respiration; international review of thoracic diseases* **76**, 288-294 (2008).

81. Corte, T.J. *et al.* Pulmonary vascular resistance predicts early mortality in patients with diffuse fibrotic lung disease and suspected pulmonary hypertension. *Thorax* **64**, 883-888 (2009).

82. Shorr, A.F., Wainright, J.L., Cors, C.S., Lettieri, C.J. & Nathan, S.D. Pulmonary hypertension in patients with pulmonary fibrosis awaiting lung transplant. *European Respiratory Journal* **30**, 715-721 (2007).

83. Lederer, D.J. *et al.* Six-minute-walk distance predicts waiting list survival in idiopathic pulmonary fibrosis. *American journal of respiratory and critical care medicine* **174**, 659-664 (2006).

84. Hayes, D., Jr. *et al.* Effect of pulmonary hypertension on survival in patients with idiopathic pulmonary fibrosis after lung transplantation: an analysis of the United

Network of Organ Sharing registry. *The Journal of heart and lung transplantation: the official publication of the International Society for Heart Transplantation* **34**, 430-437 (2015).

85. Selman, M., King, T.E. & Pardo, A. Idiopathic pulmonary fibrosis: prevailing and evolving hypotheses about its pathogenesis and implications for therapy. *Annals of internal medicine* **134**, 136-151 (2001).

86. Chambers, R.C. & Mercer, P.F. Mechanisms of alveolar epithelial injury, repair, and fibrosis. *Annals of the American Thoracic Society* **12 Suppl 1**, S16-20 (2015).

87. Cingolani, O.H. & Kass, D.A. Pressure-volume relation analysis of mouse ventricular function. *American Journal of Physiology - Heart and Circulatory Physiology* **301**, H2198-H2206 (2011).

88. Clark, J.E. & Marber, M.S. Advancements in pressure–volume catheter technology – stress remodelling after infarction. *Experimental Physiology* **98**, 614-621 (2013).

89. Voelkel, N.F., Bogaard, H.J. & Gomez-Arroyo, J. The need to recognize the pulmonary circulation and the right ventricle as an integrated functional unit: facts and hypotheses (2013 Grover Conference series). *Pulmonary circulation* **5**, 81-89 (2015).

90. Guazzi, M. *et al.* Right Ventricular Contractile Reserve and Pulmonary Circulation Uncoupling During Exercise Challenge in Heart Failure: Pathophysiology and Clinical Phenotypes. *JACC. Heart failure* **4**, 625-635 (2016).

91. Reed, W. *et al.* Production Assistance for Cellular Therapies (PACT): four-year experience from the United States National Heart, Lung, and Blood Institute (NHLBI) contract research program in cell and tissue therapies. *Transfusion* **49**, 786-796 (2009).

92. Thery, C., Amigorena, S., Raposo, G. & Clayton, A. Isolation and characterization of exosomes from cell culture supernatants and biological fluids. *Curr Protoc Cell Biol* **Chapter 3**, Unit 3 22 (2006).

93. Webber, J. & Clayton, A. How pure are your vesicles? *Journal of Extracellular Vesicles* **2**, 10.3402/jev.v3402i3400.19861 (2013).

94. Harrison, J.H., Jr. & Lazo, J.S. High dose continuous infusion of bleomycin in mice: a new model for drug-induced pulmonary fibrosis. *The Journal of pharmacology and experimental therapeutics* **243**, 1185-1194 (1987).

95. Abraham, D. & Mao, L. Cardiac Pressure-Volume Loop Analysis Using Conductance Catheters in Mice. *Journal of visualized experiments : JoVE*, 10.3791/52942 (2015).

96. Townsend, D. Measuring Pressure Volume Loops in the Mouse. e53810 (2016).

97. Tabima, D.M., Hacker, T.A. & Chesler, N.C. Measuring right ventricular function in the normal and hypertensive mouse hearts using admittance-derived pressure-volume loops.

American journal of physiology. Heart and circulatory physiology **299**, H2069-2075 (2010).

98. Maughan, W.L., Shoukas, A.A., Sagawa, K. & Weisfeldt, M.L. Instantaneous pressure-volume relationship of the canine right ventricle. *Circulation research* **44**, 309-315 (1979).

99. Faul, F., Erdfelder, E., Lang, A.G. & Buchner, A. G*Power 3: a flexible statistical power analysis program for the social, behavioral, and biomedical sciences. *Behavior research methods* **39**, 175-191 (2007).

100. Guihaire, J. *et al.* Right ventricular reserve in a piglet model of chronic pulmonary hypertension. *The European respiratory journal* **45**, 709-717 (2015).

101. Yerebakan, C. *et al.* Acute and chronic response of the right ventricle to surgically induced pressure and volume overload--an analysis of pressure-volume relations. *Interactive cardiovascular and thoracic surgery* **10**, 519-525 (2010).

102. Kass, D.A. & Kelly, R.P. Ventriculo-arterial coupling: concepts, assumptions, and applications. *Annals of biomedical engineering* **20**, 41-62 (1992).

103. Martinu, T., Palmer, S.M. & Ortiz, L.A. Lung-resident mesenchymal stromal cells. A new player in post-transplant bronchiolitis obliterans syndrome? *American journal of respiratory and critical care medicine* **183**, 968-970 (2011).

104. Sinclair, K., Yerkovich, S.T. & Chambers, D.C. Mesenchymal stem cells and the lung. *Respirology (Carlton, Vic.)* **18**, 397-411 (2013).

105. Spees, J.L., Olson, S.D., Whitney, M.J. & Prockop, D.J. Mitochondrial transfer between cells can rescue aerobic respiration. *Proc Natl Acad Sci U S A* **103**, 1283-1288 (2006).

106. Glassberg, M.K. & Toonkel, R.L. Moving stem cell therapy to patients with idiopathic pulmonary fibrosis. *Respirology (Carlton, Vic.)* **19**, 950-951 (2014).

107. Ortiz, L.A. *et al.* Mesenchymal stem cell engraftment in lung is enhanced in response to bleomycin exposure and ameliorates its fibrotic effects. *Proceedings of the National Academy of Sciences of the United States of America* **100**, 8407-8411 (2003).

108. Cocucci, E., Racchetti, G. & Meldolesi, J. Shedding microvesicles: artefacts no more. *Trends Cell Biol* **19**, 43-51 (2009).

109. Witwer, K.W. *et al.* Standardization of sample collection, isolation and analysis methods in extracellular vesicle research. *J Extracell Vesicles* **2** (2013).

110. Lai, R.C. *et al.* Exosome secreted by MSC reduces myocardial ischemia/reperfusion injury. *Stem cell research* **4**, 214-222 (2010).

111. Russell, K.C. *et al.* In vitro high-capacity assay to quantify the clonal heterogeneity in trilineage potential of mesenchymal stem cells reveals a complex hierarchy of lineage commitment. *Stem Cells* **28**, 788-798 (2010).

112. Pickering, A.M. & Davies, K.J. Degradation of damaged proteins: the main function of the 20S proteasome. *Progress in molecular biology and translational science* **109**, 227-248 (2012).

113. Figeys, D. Proteomics: the basic overview. *Methods of biochemical analysis* **45**, 1-62 (2005).

114. Kim, H.S. *et al.* Proteomic analysis of microvesicles derived from human mesenchymal stem cells. *Journal of proteome research* **11**, 839-849 (2012).

115. Anderson, J.D. *et al.* Comprehensive Proteomic Analysis of Mesenchymal Stem Cell Exosomes Reveals Modulation of Angiogenesis via Nuclear Factor-KappaB Signaling. *Stem cells (Dayton, Ohio)* **34**, 601-613 (2016).

116. Haraszti, R.A. *et al.* High-resolution proteomic and lipidomic analysis of exosomes and microvesicles from different cell sources. *Journal of extracellular vesicles* **5**, 32570 (2016).

117. Kowal, J. *et al.* Proteomic comparison defines novel markers to characterize heterogeneous populations of extracellular vesicle subtypes. *Proceedings of the National Academy of Sciences of the United States of America* **113**, E968-977 (2016).

118. Tkach, M., Kowal, J. & Thery, C. Why the need and how to approach the functional diversity of extracellular vesicles. *Philosophical transactions of the Royal Society of London. Series B, Biological sciences* **373** (2018).

119. Kanehisa, M., Sato, Y., Kawashima, M., Furumichi, M. & Tanabe, M. KEGG as a reference resource for gene and protein annotation. *Nucleic acids research* **44**, D457-462 (2016).

120. Kanehisa, M. Enzyme Annotation and Metabolic Reconstruction Using KEGG. *Methods in molecular biology (Clifton, N.J.)* **1611**, 135-145 (2017).

121. Schmidt, A., Forne, I. & Imhof, A. Bioinformatic analysis of proteomics data. *BMC systems biology* **8 Suppl 2**, S3 (2014).

122. Wood, D. *et al.* An update from the United States National Heart, Lung, and Blood Institute-funded Production Assistance for Cellular Therapies (PACT) program: a decade of cell therapy. *Clinical and translational science* **7**, 93-99 (2014).

123. Hendrickson, R.C. *et al.* High-Resolution Discovery Proteomics Reveals Candidate Disease Progression Markers of Alzheimer's Disease in Human Cerebrospinal Fluid. *PloS one* **10**, e0135365 (2015).

124. Benjamini, Y. & Hochberg, Y. Controlling the False Discovery Rate: A Practical and Powerful Approach to Multiple Testing. *Journal of the Royal Statistical Society. Series B (Methodological)* **57**, 289-300 (1995).

125. Kall, L., Storey, J.D., MacCoss, M.J. & Noble, W.S. Assigning significance to peptides identified by tandem mass spectrometry using decoy databases. *Journal of proteome research* **7**, 29-34 (2008).

126. Yi, M. & Stephens, R.M. SLEPR: a sample-level enrichment-based pathway ranking method -- seeking biological themes through pathway-level consistency. *PloS one* **3**, e3288 (2008).

127. Evangelou, M., Rendon, A., Ouwehand, W.H., Wernisch, L. & Dudbridge, F. Comparison of methods for competitive tests of pathway analysis. *PloS one* **7**, e41018 (2012).

128. Lenfant, N., Hotelier, T., Bourne, Y., Marchot, P. & Chatonnet, A. Proteins with an alpha/beta hydrolase fold: Relationships between subfamilies in an ever-growing superfamily. *Chemico-biological interactions* **203**, 266-268 (2013).

129. Merino-Gonzalez, C. *et al.* Mesenchymal Stem Cell-Derived Extracellular Vesicles Promote Angiogenesis: Potencial Clinical Application. *Frontiers in physiology* **7**, 24 (2016).

130. Piao, L., Marsboom, G. & Archer, S.L. Mitochondrial metabolic adaptation in right ventricular hypertrophy and failure. *Journal of Molecular Medicine* **88**, 1011-1020 (2010).

131. Fazzi, F. *et al.* TNFR1/phox interaction and TNFR1 mitochondrial translocation Thwart silica-induced pulmonary fibrosis. *Journal of immunology (Baltimore, Md.: 1950)* **192**, 3837-3846 (2014).

132. Yi, H. *et al.* Exosomes mediated pentose phosphate pathway in ovarian cancer metastasis: a proteomics analysis. *International journal of clinical and experimental pathology* **8**, 15719-15728 (2015).